

Mpemba meets quantum chaos: Anomalous relaxation and Mpemba crossings in dissipative Sachdev-Ye-Kitaev models

Xuanhua Wang,^{1,*} Jie Su,^{1,†} and Jin Wang^{1,2,3,‡}

¹*Center for Theoretical Interdisciplinary Sciences, Wenzhou Institute,*

University of Chinese Academy of Sciences, Wenzhou, Zhejiang 325001, China

²*Department of Chemistry, Stony Brook University, Stony Brook, New York 11794, USA*

³*Department of Physics and Astronomy, Stony Brook University, Stony Brook, New York 11794, USA*

The Mpemba effect (MPE), named after a student who first observed the phenomenon, has intrigued scientists for decades by showing that hot liquid can freeze faster than cold under certain conditions. Recently, analogous effects have been identified in integrable quantum systems. However, a key distinction between the classical MPE and its quantum analog is that the latter relies predominantly on the properties of the initial states rather than the cooling rate. In this paper, we explore the quench dynamics of Sachdev-Ye-Kitaev (SYK) systems coupled to thermal baths. We investigate three scenarios—SYK systems coupled to SYK thermal baths, SYK systems coupled to two thermal baths at different temperatures, and dissipative SYKs modeled by the Lindblad equation. In the regimes where the system and the baths are strongly coupled, we observe effective temperature oscillations and Mpemba crossings (MPCs)—the effect of temperature crossings which are absent in quasi-equilibrium thermodynamic analysis—when the system is strongly coupled to SYK thermal baths. These effects are not observed in the Liouvillian formalism. The emergence of MPCs in quantum chaotic systems exhibits strong parallels with the classical MPE.

I. INTRODUCTION

The Mpemba effect (MPE) originates from a classroom experiment by a student named Mpemba, who discovered that hot milk could freeze faster than cold milk. This effect challenges conventional knowledge of thermodynamics and has garnered significant attention in recent years due to its counterintuitive nature. Despite early skepticism stemming from a lack of rigorous experimental controls, recent advancements in experimental techniques have facilitated more precise investigations. Observations of the Mpemba effects in various systems, including water [1], granular fluids [2, 3], molecular gases [4, 5], and ion-trap quantum computers [6, 7], have further fueled interest in understanding its conditions for emergence as well as the underlying mechanisms [8]. Furthermore, observations of similar dynamic anomalies have expanded the scope of the original MPE to include dynamical trajectory crossings of any observable that would not intersect in quasi-equilibrium limit. Such crossings, absent in equilibrium thermodynamic analyses, are referred to as the Mpemba crossings (MPCs) [9–11].

While disputes still exist around the reproducibility and predicability of classical MPEs [12, 13], recent research in quantum systems has shed light on this problem. Quantum systems, such as spin chains and few-body systems, have exhibited numerous anomalous dynamics analogous to the classical MPE [11, 14–21]. The most investigated quantum systems among them are the integrable systems governed by relatively simple Hamiltonians such as minimal Kitaev model and quantum dot model, whose system dynamics are approximated by the Lindblad equation, incorporating the non-unitary dissipation. Despite the progress made by the studies, criticisms still remain. One is that the degree of nonequilibrium, which is the key to the emergence of MPEs in classical systems, is not the determinant factor in these simple integrable systems. Furthermore, one may question that for an N -level quantum system weakly interacting with the environment, the MPE may not be so bizarre since one can always prepare the initial state of the system to be the fast-decaying mode in the Liouvillian spectrum. To be specific, for an N -level open quantum system, the Liouvillian equation of motion for the linearized density matrix $\vec{\rho}$ is approximately

$$\frac{d\vec{\rho}(t)}{dt} = \mathcal{L}_{T_b}\vec{\rho}_0. \quad (1)$$

Then, one can always pick the particular initial state ρ_{fast} such that its inner product with the slowest decaying eigen mode of the superoperator \mathcal{L}_{T_b} vanishes [see Fig. 1]. It is natural to conclude from the above argument that the key to the emergence of the MPE is the peculiarity of the initial states rather than the degree the system is driven out of equilibrium or the cooling rate. Consequently, it raises concern whether the MPEs in quantum integrable models are fundamentally related to the classical MPE, which is highly dependent on the rate of cooling. In an infinitely slow cooling process, a system can be well-described by equilibrium thermodynamics and the classical MPE does not appear. Besides, such simplistic arguments may not even be

* Corresponding author: wangxh@ucas.ac.cn

† Co-first author.

‡ Corresponding author: jin.wang.1@stonybrook.edu

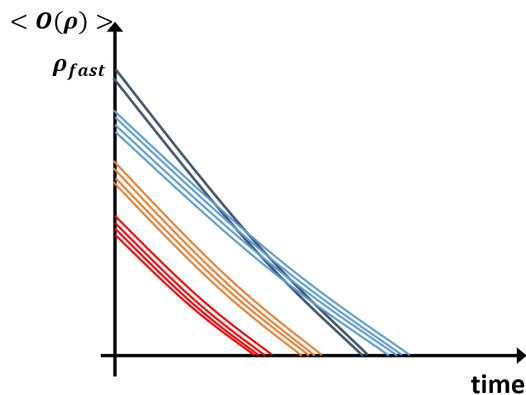


FIG. 1. In quantum systems with discrete Liouvillian eigenmodes, the presence of fast-decaying modes (the black curves) determines the emergence of the MPE for the observable $O(\rho)$. In such cases, the MPE typically depends on whether the initial state largely overlaps with the fast modes. Consequently, the emergence of the MPE relies more on the initial conditions of the state rather than on how rapidly the system is cooled.

naively extended to more complex quantum systems such as those exhibiting quantum chaos. The information about a finely tuned initial state is rapidly scrambled and washed away, for instance, by the randomness in the ensembles of Hamiltonians and the chaotic dynamics [22, 23]. As a result, the MPE does not easily emerge for the same reason as in integrable models. To exploit the simplicity of quantum systems while with aiming to gain insight into MPEs in complex classical systems, the most relevant models to investigate are quantum chaotic systems. Quantum chaos, defined as the behavior of a quantum system whose classical limit is chaotic [22, 24, 25], provides a crucial link between simple quantum dynamics and complex classical behavior.

The Sachdev-Ye-Kitaev (SYK) model, featured by its quantum chaotic nature, stands as an optimal entry point for addressing the aforementioned issues [26, 27]. The SYK model originates from the Sachdev-Ye (SK) model, which was initially conceived to investigate many-body chaos in spin- S Heisenberg models [28]. The calculation of the two-point Green's functions of fermionic models with random coupling strengths following Gaussian distributions revealed the spin glass ground states in the large- S limit and the emergence of scale-invariant behavior under finite- S conditions. Subsequently, Kitaev extended this theory further, demonstrating that the dynamics of similar models at low temperatures can be described by Schwarzian equations [29]. The SYK model established the duality between the dynamics of N -body systems with long-range random interactions of Majorana fermions at low energies and Jackiw-Teitelboim (JT) gravity dynamics. SYK model emerges as an example of a solvable model that demonstrates strongly coupled quantum many-body phenomena and displays the properties of holographic quantum matter without quasi-particle excitations. Furthermore, it was found that the upper bound of the Lyapunov constant, describing black hole chaos, precisely corresponds to the SYK model, offering new insights into quantum gravity in low dimensions [22, 24, 27, 30, 31]. For instance, it was shown that the dominant term in the gravitational dual of two weakly coupled SYK models at low temperatures is a traversable wormhole, while at higher temperatures, the dominant contribution comes from the black hole configuration [32–35]. Notably, the real-time Hamiltonian dynamics as well as the quench dynamics of an open SYK model coupled to an external bath have been explored [32, 34, 36–45]. In particular, the dissipative SYK models have similar feature of quantum chaos but with slightly reduced Lyapunov exponents depending on the coupling strength with the bath [36, 46]. In the SYK model, due to the random Gaussian distribution of interaction strengths, whether anomalous dynamics such as MPEs will emerge is no longer evident, and its mechanisms may be fundamentally different from that in integrable systems.

In this study, we explore the anomalous dynamics and MPCs in the quench dynamics of SYK models coupled to thermal baths. While previous studies have examined SYK quench dynamics under weak system-bath coupling [37, 39, 42, 43], showing that the effective temperature at late times follows a smooth relaxation process without the emergence of MPCs, we focus on the behavior under strong coupling conditions. In weakly coupled cases, the effective temperature of the SYK at late times approximately follows

$$\beta_{\text{eff}}(t) = \beta_f + \alpha \exp(-\Gamma t), \quad (2)$$

where β_f is the temperature at the final state, α is related to the temperature difference between the initial and the final states, and Γ is the thermalization rate independent of the initial state [39]. This formula predicts no such emergence as MPCs. However, under strong coupling for the SYK model set to couple to a large SYK bath at $t = 0$, we observe transient overcooled and overheated phases, with oscillations around the steady-state temperature once the coupling exceeds certain threshold. Additionally, we compare the dynamics of open SYK models derived from the two different formalisms—SYKs coupled with SYK baths

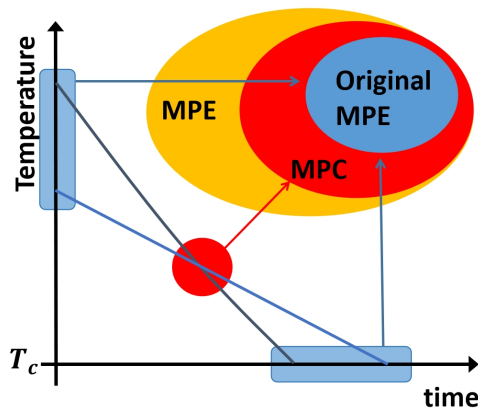


FIG. 2. Diagrammatic illustration of MPEs and MPCs. The original MPE describes the phenomenon that the higher- and the lower-temperature states switch relative positions at certain critical temperature T_c , usually corresponding to the bath or some phase transition temperature such as the icing point. The original MPE is only defined by the initial conditions and the final states at T_c (the blue shaded regions along the x- and y-axes). An MPC refers to the crossing of the temperature trajectories before reaching the steady state as indicated by the red circled region at the intersection of the two curves. The generalized MPE, abbreviated as MPE for simplicity and represented by the orange circled region, encompasses the emergence of MPCs, including the emergence of multiple MPCs in rapid relaxations, and requires analysis of the trajectory data during the entire cooling or heating dynamics.

and the dissipative SYK Lindbladian. In contrast to the SYK-bath coupling, the dynamics derived from the Lindbladian do not manifest any anomalous behaviors. We offer a possible reason for this difference.

II. QUANTUM MPES AND MPES

In recent years, MPEs in quantum systems have garnered significant attention. Among the most investigated topics are the dynamics of chosen observables, in particular, the entanglement symmetry restoration [9, 18–20, 47], and the so-called Markovian quantum MPEs [8, 11, 14, 16, 17, 48].

The anomalous trajectory crossings of chosen measures such as entanglement asymmetry and trace distance between two initial states have been considered analogous to the classical MPE. Nevertheless, the differences between them should not be overlooked. One can demystify the MPEs in the entanglement symmetry restoration by noticing that the state further from the steady state, as measured by entanglement asymmetry, is not necessarily the state further away from the steady state in the thermalization process. In fact, the original MPE points to anomalies in thermalization dynamics, while the quantum MPE related to entanglement asymmetry reflects an anomaly in the entanglement measure itself. Specifically, states that thermalize to equilibrium faster can still display larger entanglement asymmetries. This quantum MPE sidesteps the original problem of thermalization dynamics by shifting focus to a different measure—entanglement asymmetry—yet the broader question of anomalous thermalization remains. For the Markovian MPE, it can be attributed to different decay rates of eigen modes and the overlaps between the initial states and the slowest mode. Therefore, in both cases, the emergence of the MPEs relies on the peculiarity of the initial state and the property of the chosen measure. However, unlike in classical systems—where MPEs vanish under infinitely slow cooling and quasi-equilibrium thermodynamics—in quantum systems, the nonequilibrium dynamics are not as decisive. The key difference from the original MPE is that in the classical MPE, if the cooling process is infinitely slow such that the system can be treated by equilibrium thermodynamics, MPEs will not emerge. While in the above cases of the quantum analog, the nonequilibriumness of the system does not play such a decisive role.

Originally, the MPE refers to the emergence of a single anomalous temperature crossing, or an MPC, in the cooling dynamics, so that the relative positions of the effective temperatures are switched when the system is measured at a designated temperature T_c —the icing point in the original Mpemba experiment [see Fig. 2 for diagrammatic illustration]. Typically, this designated temperature is the temperature of a phase transition or the asymptotic temperature of the steady state. However, for systems driven even further away from the equilibrium than the Mpemba system in its original conception, the temperature trajectories can have additional crossing below T_c . Up to now, the concept of the MPE has been generalized to include not only the dynamics that has one or an odd number of MPCs so that the malposition of temperatures can be observed at T_c , but also the dynamics that has an even number of MPCs, in which transient anomalies can be detected in the intermediate state rather than at the final state. In fact, MPC is deeply related to the originally proposed MPE in the icing process of hot liquid as in both cases the temperatures in the cooling processes are understood as the effective temperatures and one monitor the effective temperatures during the entire cooling (heating) processes and claim the detection of the MPE once an MPC is found. The MPC is one of

the distinctive manifestations of dynamical anomalies beyond the quasi-equilibrium characterization. It is a feature of a strongly nonequilibrium system and is driven by rapid relaxation. The MPC monitors the entire dynamics of the system and provides a refined characterization of the dynamical anomaly beyond the original MPE, which only needs data regarding the initial and the final states. In this study, we argue that the MPCs found in the quantum chaotic systems share more similarities with the original MPE and originate from the same underlying mechanism in contrast to quantum MPEs found in many quantum integrable models.

III. SYK MODELS IN THERMAL BATHS

A. SYK model in a thermal bath

We consider a q -body interacting SYK $_q$ model in a thermal bath, consisting of N Majorana fermions in (0+1) dimensions with random q -fermion interactions. The bath is also an SYK $_q$ model governed by the same Hamiltonian with N^2 Majorana modes. In the large- N and weak system-bath coupling limits, the model exhibits maximal chaos for $q > 2$, saturating the bound on the quantum Lyapunov exponent derived from out-of-time-ordered correlators. For simplicity, we focus on $q = 4$ case and the total Hamiltonian is given by

$$H = H_{\text{SYK}}[J_{i_1 i_2 i_3 i_4}, \chi] + H_{\text{SYK}}[\tilde{J}_{i_1 i_2 i_3 i_4}, \psi] + \sum_{a i_1 i_2 \dots i_n} \frac{V_{a i_1 i_2 \dots i_n}}{n!} \chi_a \psi_{i_1} \psi_{i_2} \dots \psi_{i_n}. \quad (3)$$

where χ_i are the Majorana fermions of the system on site $i = 1 \dots N$ obeying

$$\{\chi_i, \chi_j\} = \delta_{ij}, \quad (4)$$

and ψ_i represent the bath operators on site $i = 1 \dots N^2$. $H_{\text{SYK}}[J_{i_1 i_2 i_3 i_4}, \chi]$ and $H_{\text{SYK}}[\tilde{J}_{i_1 i_2 i_3 i_4}, \psi]$ are the standard SYK $_4$ Hamiltonians for the system (χ) and the bath (ψ), respectively, which are given by

$$H_{\text{SYK}}[J_{i_1 i_2 i_3 i_4}, \chi] = \sum_{i_1 i_2 i_3 i_4} \frac{J_{i_1 i_2 i_3 i_4}}{4!} \chi_{i_1} \chi_{i_2} \chi_{i_3} \chi_{i_4}, \quad (5)$$

$$H_{\text{SYK}}[\tilde{J}_{i_1 i_2 i_3 i_4}, \psi] = \sum_{i_1 i_2 i_3 i_4} \frac{\tilde{J}_{i_1 i_2 i_3 i_4}}{4!} \psi_{i_1} \psi_{i_2} \psi_{i_3} \psi_{i_4}. \quad (6)$$

The distributions of the interaction strengths are given by:

$$\overline{J_{i_1 i_2 i_3 i_4}} = 0, \quad \overline{\tilde{J}_{i_1 i_2 i_3 i_4}} = 0, \quad \overline{V_{a i_1 i_2 \dots i_n}} = 0, \quad (7)$$

$$\overline{J_{i_1 i_2 i_3 i_4}^2} = \frac{3!J^2}{N^3}, \quad \overline{\tilde{J}_{i_1 i_2 i_3 i_4}^2} = \frac{3!J^2}{N^6}, \quad \overline{V_{a i_1 i_2 \dots i_n}^2} = \frac{n!V^2}{N^{2n}}. \quad (8)$$

For a non-interacting SYK model in equilibrium with the time translation symmetry, the Euclidean Green's function at the zero-temperature limit is

$$G_\psi(\tau) = \langle T(\psi(\tau)\psi(0)) \rangle = \langle \psi(\tau)\psi(0) \rangle \theta(\tau) - \langle \psi(0)\psi(\tau) \rangle \theta(-\tau) = b_\psi \frac{\text{sgn}(\tau)}{|\tau|^{1/2}}, \quad 4\pi J^2 b_\psi^4 = 1, \quad (9)$$

and the Green's function at finite temperature is given by conformal mapping $\tau = \tan \frac{\pi\tau'}{\beta}$ [26]. This gives the correlation function at the inverse temperature β

$$G_\psi(\tau) = b_\psi \frac{\text{sgn}(\tau) \pi^{1/2}}{(\beta \sin \frac{\pi\tau}{\beta})^{1/2}}, \quad 4\pi J^2 b_\psi^4 = 1. \quad (10)$$

From the Euclidean correlators, we can obtain the zero- and finite-temperature correlators in Lorentzian time by setting $\tau = it$ [26], which gives

$$G_\psi(t) = b_\psi \frac{e^{-i\pi/4}}{t^{1/2}} \text{sgn}(t), \quad G_\psi(t, \beta) = b_\psi \frac{\text{sgn}(t) e^{-i\pi/4} \pi^{1/2}}{(\beta \sinh \frac{\pi t}{\beta})^{1/2}}, \quad (11)$$

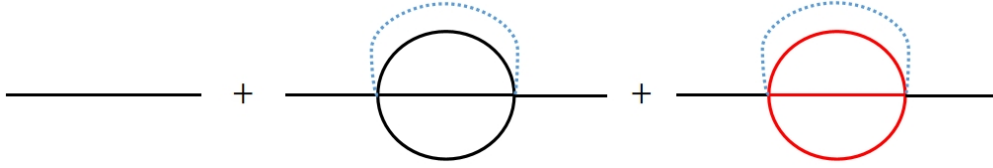


FIG. 3. Leading-order corrections to the two-point function of the system SYK $_{\chi}$ for $q = 4$, $n = 3$. The solid black line represents the correlator of the Majorana fermion χ . The red line represents the correlator of the bath fermion ψ . The dotted line represents the disorder averaging that identifies the coupling constants of the connected vertices. The diagrams can be summed by computing the self consistency equations of the propagator and self energy. The self energy Σ includes all the one particle irreducible contributions to the propagator.

where $G_{\psi}(t)$ is the Lorentzian correlator at zero temperature and $G_{\psi}(t, \beta)$ is the Lorentzian correlator at temperature β^{-1} . For the interacting SYK model with Hamiltonian given by Eq. (3), the Green's function can be read directly from Fig. 3:

$$G_{\chi}^{-1}(\omega_n) = -i\omega_n - \Sigma_{\chi}(\omega_n), \quad (12)$$

$$\Sigma_{\chi}(\tau) = J^2 G_{\chi}(\tau)^3 + V^2 G_{\psi}(\tau)^n. \quad (13)$$

In the diagrammatic representation Fig. 3, only contributions of order N^0 are presented.

In real time, the quench dynamics can be analysed on the Keldysh contour where fields with subscripts “-” signs (e.g. ψ_-) live on the lower contour C_- and fields with subscripts “+” signs live on the upper contour C_+ as shown in Fig. 4. In this case, the self-energy for the system can be written as

$$\begin{aligned} \hat{\Sigma}_{\chi, \alpha\beta}(t, t') &\equiv \begin{pmatrix} \Sigma_{\chi}^T(t, t') & -\Sigma_{\chi}^<(t, t') \\ -\Sigma_{\chi}^>(t, t') & \Sigma_{\chi}^T(t, t') \end{pmatrix}_{\alpha\beta} \\ &= -J^2 \alpha\beta G_{\chi, \alpha\beta}^3(t, t') - V^2 \alpha\beta (-1)^{\frac{n+1}{2}} \theta(t)\theta(t') G_{\psi, \alpha\beta}^n(t, t'), \end{aligned} \quad (14)$$

where α and β are + and - signs. Similarly, the self-energy for the bath is:

$$\begin{aligned} \hat{\Sigma}_{\psi, \alpha\beta}(t, t') &\equiv \begin{pmatrix} \Sigma_{\psi}^T(t, t') & -\Sigma_{\psi}^<(t, t') \\ -\Sigma_{\psi}^>(t, t') & \Sigma_{\psi}^T(t, t') \end{pmatrix}_{\alpha\beta} \\ &= -J^2 \alpha\beta G_{\psi, \alpha\beta}^3(t, t'). \end{aligned} \quad (15)$$

The correlators defined on the Keldysh contours can be viewed as a two-by-two matrix in the 2D space of the contour branch indices [49] such as

$$\hat{G}_{\chi, \alpha\beta}(t, t') = -i \langle \mathbf{T}_c \chi_{\alpha}(t) \chi_{\beta}(t') \rangle = \begin{pmatrix} G_{\chi}^T(t, t') & G_{\chi}^<(t, t') \\ G_{\chi}^>(t, t') & G_{\chi}^T(t, t') \end{pmatrix}, \quad (16)$$

where $\alpha, \beta = \pm$, $G_{\chi}^T(t, t') = \theta(t-t')G_{\chi}^>(t, t') + \theta(t'-t)G_{\chi}^<(t, t')$ and $G_{\chi}^T(t, t') = \theta(t'-t)G_{\chi}^>(t, t') + \theta(t-t')G_{\chi}^<(t, t')$. The symbol \mathbf{T}_c denotes the contour ordering of the operators such that they are arranged from right to left in the same order as their sequence along the contour. For example, $\mathbf{T}_c \chi(t_1^+) \chi(t_2^-) = \xi \chi(t_2^-) \chi(t_1^+)$, where $\xi = 1$ for bosonic operators and $\xi = -1$ for fermionic operators.

From the above definition, it is easy to read the averaged “greater” and “lesser” Green's functions, which are the correlators of the fields living on two different contours defined as follows:

$$G^>(t_1, t_2) \equiv G(t_1^-, t_2^+) = \frac{-i}{N} \sum_{i=1}^N \langle \psi(t_1^-) \psi(t_2^+) \rangle \quad (17)$$

$$G^<(t_1, t_2) \equiv G(t_1^+, t_2^-) = \frac{i}{N} \sum_{i=1}^N \langle \psi(t_2^-) \psi(t_1^+) \rangle. \quad (18)$$

The lesser and greater correlation functions are independent functions for Dirac (complex) fermions. For the Majorana fermions, it is straightforward from above equations that

$$G^>(t, t') = -G^<(t', t), \quad (19)$$

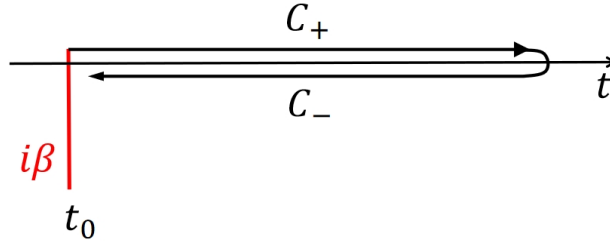


FIG. 4. Demonstration of the Keldysh contour used in this study. The upper and lower contours are denoted by C_+ and C_- , respectively. The thermal state is prepared at the time $t_0 \ll 0$.

which holds even for nonequilibrium dynamics. For states in thermal equilibrium or in general states evolved from thermal equilibrium states, the greater and lesser function satisfies $G^>(t, t') = (G^<(t, t'))^*$ [38, 49]. Therefore, $G^>(t_1, t_2) = -(G^>(t_2, t_1))^*$. In this formalism, sometimes it is more convenient to write the equations in the Keldysh basis, where the retarded, advanced and Keldysh correlators are defined as follows:

$$G_R(t, t') = \theta(t - t')(G^>(t, t') - G^<(t, t')), \quad (20)$$

$$G_A(t, t') = \theta(t' - t)(G^<(t, t') - G^>(t, t')), \quad (21)$$

$$G_K(t, t') = G^<(t, t') + G^>(t, t'). \quad (22)$$

The above definitions will be used later.

B. Equilibrium solutions

In this section, we briefly summarize the procedures to obtain the exact equilibrium Green's function of the system when interactions with the bath considered. The Green's function is obtained by solving the Dyson's equation self-consistently starting from the initial input which is set to the conformal limit of the thermal Green's function. One may refer to ref. [39] for details.

Since the equilibrium solution of the Green's function has the time translational symmetry, the Green's function $G_{\alpha,\beta}(t_1, t_2)$ is only dependent on the relative time $t = t_1 - t_2$ and is abbreviated as $G_{\alpha,\beta}(t)$. In thermal equilibrium, the Kubo–Martin–Schwinger condition gives [50]

$$G^>(\omega) = \pm e^{\beta\omega} G^<(\omega), \quad (23)$$

where the + sign is for bosons and – sign is for fermions. The spectral function

$$A(\omega) = -2\text{Im}G_R(\omega) \quad (24)$$

can be determined by the self-consistent equation of retarded Green's functions. In thermal equilibrium, the greater Green's function is related to the spectral function by

$$G^>(\omega) = -i(1 - n_F(\omega, T)) = -in_F(-\omega, T)A(\omega), \quad (25)$$

where $n_F(\omega, T)$ is the Fermi-Dirac distribution function given by $n_F = \frac{1}{1+e^{\beta\omega}}$. For Majorana fermions, the operators satisfy $\psi^\dagger = \psi$ and the Green's function satisfies:

$$G(-t) = -G^*(t), \quad (26)$$

one can obtain the retarded Green's function in the conformal limit [26]:

$$iG^R(t) = \theta(t)\langle[(\psi(t), \psi(0))]\rangle = 2b \cos(\pi/q) \left(\frac{\pi}{\beta \sinh(\frac{\pi t}{\beta})} \right)^{\frac{2}{q}} \theta(t), \quad (27)$$

where time translational symmetry is assumed. The retarded Green's function in Eq. (27) can be used as a proper choice of the initial data for generating the exact Green's function through the iteration to be described below. Adopting the following

convention for the Fourier transformations:

$$A(\omega) = \int_{-\infty}^{\infty} dt A(t) e^{i\omega t}, \quad (28)$$

$$A(t) = \int_{-\infty}^{\infty} \frac{d\omega}{2\pi} A(\omega) e^{-i\omega t}, \quad (29)$$

we have the self-consistency equations:

$$\begin{aligned} G_R(\omega)^{-1} &= \omega - \Sigma_R(\omega), \\ \Sigma_R(\omega) &= -iJ^2 \int_0^{\infty} dt e^{i\omega t} (n(t)^3 + (n(t)^*)^3), \\ n(t) &= \int \frac{d\omega}{2\pi} e^{-i\omega t} A(\omega) n_F(\omega, T). \end{aligned} \quad (30)$$

The exact Green's function of the SYK model in thermal equilibrium can be computed numerically by iterating Eqs.(24), (25) and (30) until the solution converges. The solutions are used for the initial conditions of the SYK system and the baths.

C. Definitions of temperature

To capture the statistical property of the out-of-equilibrium system after the quench, we track the effective temperature changes with time. For systems out of thermal equilibrium, temperature is not evidently and uniquely defined as in equilibrium systems. Instead, observables such as the effective temperatures are defined to reflect the overall statistical properties of the system and serve as trackers for the possible emergence of the MPE. We consider the diagonal slices of the Green's function $G^>(t_1, t_2)$,

$$G_d^>(t; t') = G^>(t + t', t - t'), \quad (31)$$

then apply the fluctuation-dissipation theorem (FDT) [50–52] to find the effective temperature at time t :

$$\frac{\text{Im}(G^>(\omega, t) + G^<(\omega, t))}{\text{Im}(G^R(\omega, t))} = -\tanh \frac{\beta(t)\omega}{2}, \quad (32)$$

where the Green's function $G(\omega, t)$ in the above equation is defined through Wigner transformation [53]

$$G(\omega, t) = \int_0^{\infty} dt' e^{i\omega t'} G(t + t'/2, t - t'/2). \quad (33)$$

Therefore, the inverse of the effective temperature can be expressed as [39]

$$\beta(t) = \frac{2 \cdot \text{Im}(G_{\chi,K}(\omega, t))}{\omega \cdot \text{Im}(G_{\chi,R}(\omega, t))} \Big|_{\omega \rightarrow 0}. \quad (34)$$

This definition preserves the FDT but suffers from the possible ailment of causality violation in time [54]. Another possible way to characterize the transient effective temperature of the system after the quench is through the corner slice of the Green's function [40]:

$$G_c^>(t, t') = \theta(t') G^>(t - t', t) + \theta(-t') G^>(t, t + t'). \quad (35)$$

Then, we can similarly define $G_c^>(\omega, t)$ by Fourier transforming $G_c^>(t, t')$ on t' , i.e.,

$$G_c^>(\omega, t) = \int_{-\infty}^{\infty} dt' e^{i\omega t'} G(t, t'). \quad (36)$$

One can then define the inverse temperature by inserting the above definition of $G_c^{>(<)}$ (ω, t) into the expression below [55]

$$\beta'(t) = \frac{-\text{Im}(G_{\chi,K}(\omega, t))}{\omega \cdot \text{Im}(G_{\chi,R}(\omega, t))} \Big|_{\omega \rightarrow 0}. \quad (37)$$

As remarked in ref. [40], this definition respects the causality but at the expense of the FDT violation at higher frequencies. For this study, we ignore possible issues with the characterization of the effective temperatures of nonequilibrium systems and treat them as certain statistical measures to detect the emergence of the MPE. We remark that these two quantities may differ slightly when the system is away from the equilibrium but qualitatively very similar and agree exactly when the system is in thermal equilibrium. The conclusions in this study are independent of which definition we use. For simplicity, the definition by Eq. (34) is what we will mainly refer to in this study.

D. Kadanoff-Baym equation and quench dynamics

The dynamics of the SYK system after the quench can be described by the Kadanoff-Baym equations, i.e., the equations of motion of the system. In these equations, the influence of the bath on the SYK model is of order one, while the influence of the SYK model on the self energy of the bath is of higher orders in the large- N expansion and can be ignored. We solve the Kadanoff-Baym equation numerically. For the SYK systems in the thermal bath, we need to solve for $G_\chi^>(t, t')$ and $G_\chi^<(t, t')$. For $t, t' < 0$, the system is prepared to a thermal equilibrium state and the Green's functions satisfy, viz., $G_\chi^>(t, t') = G_\chi^>(t - t')$, where we have assumed the time translational invariance. The data can be easily discretized and stored in terms of $\{\Delta t, G_\chi^>(\Delta t)\}$ as the initial condition for numerical simulations of the quench dynamics.

The retarded, advanced and Keldysh components of the self-energy are defined in a similar way as that for the Green's function, viz.,

$$\Sigma_R(t, t') = \theta(t - t')(\Sigma^>(t, t') - \Sigma^<(t, t')), \quad (38)$$

$$\Sigma_A(t, t') = \theta(t' - t)(\Sigma^<(t, t') - \Sigma^>(t, t')), \quad (39)$$

$$\Sigma_K(t, t') = \Sigma^<(t, t') + \Sigma^>(t, t'). \quad (40)$$

For the Majorana fermions, the greater and lesser Green's functions satisfy the relation $G^>(t, t') = (G^<(t, t'))^*$. Using the Langreth rule [50], we integrate the Schwinger-Dyson equation and obtain the Kadanoff-Baym equations for the Green's functions of the SYK system given as follows:

$$i\partial_{t_1} G_\chi^>(t_1, t_2) = \int dt_3 (\Sigma_\chi^R(t_1, t_3) G_\chi^>(t_3, t_2) + \Sigma_\chi^>(t_1, t_3) G_\chi^A(t_3, t_2)), \quad (41)$$

$$-i\partial_{t_2} G_\chi^>(t_1, t_2) = \int dt_3 (G_\chi^R(t_1, t_3) \Sigma_\chi^>(t_3, t_2) + G_\chi^>(t_1, t_3) \Sigma_\chi^A(t_3, t_2)), \quad (42)$$

where the self-energies for the SYK₄ system denoted by χ and for the bath denoted by ψ are defined as follow:

$$\Sigma_\chi^>(t, t') = -J^2 (G_\chi^>(t, t'))^3 - V^2 (-1)^{\frac{n+1}{2}} \theta(t)\theta(t') (G_\psi^>(t, t'))^n, \quad (43)$$

$$\Sigma_\chi^<(t, t') = -J^2 (G_\chi^<(t, t'))^3 - V^2 (-1)^{\frac{n+1}{2}} \theta(t)\theta(t') (G_\psi^<(t, t'))^n, \quad (44)$$

$$\Sigma_\psi^<(t, t') = -J^2 (G_\psi^<(t, t'))^3, \quad (45)$$

$$\Sigma_\psi^>(t, t') = -J^2 (G_\psi^>(t, t'))^3. \quad (46)$$

Then, we numerically solve Eqs. (41) and (42) by discretizing (t_1, t_2) into a 1000×1000 lattice with size Δt . The differential equations become the difference equations and the integration can be approximated by summation, and $G_\chi^>$ in the steady state can be simulated by the iterative method. First, we need to get the initial state at each different initial temperature $1/\beta_i$, where the data of on-lattice $G_\chi^>(t_1, t_2)$ can be obtained from the equilibrium solution. Then the difference of $G_\chi^>$ on each lattice $(\Delta_{t_1} G_\chi^>, \Delta_{t_2} G_\chi^>)$ can be calculated from the summation approximated by Eqs. (41) and (42), and we can naturally update the data of $G_\chi^>$ based on the difference. Repeat calculations of the difference and updating of $G_\chi^>$ until $G_\chi^>$ maintains unchanged with time, i.e., the difference of $G_\chi^>$ decay to 0. In simulation, we choose $J = 0.5$ and the cutoff in the time domain $\Lambda_t = 50$, and thus restrict t to $[-\Lambda_t, \Lambda_t]$ so that $\Delta t = 0.1$. To ensure the accuracy of the simulated results, especially to avoid the size effects, we have augmented the number of lattice to 2000×2000 . Furthermore, we have modulated the parameter Λ_t to either 100 (corresponding to $\Delta t = 0.1$) or maintained it at 50 (corresponding to $\Delta t = 0.05$). The quantitative results obtained under these parameter settings exhibit a high degree of consistency with those derived using the selected parameters, thereby validating the accuracy of our simulations. Then, we use the data of the Green's function to compute the dynamics of the inverse of the effective temperature.

E. Numerical results for SYKs in a thermal bath

It is usually expected that during cooling processes, the temperature of a SYK model exponentially approaches its asymptotic temperature which is determined by its environment. However, we find that the system temperature after the quench shows an oscillatory feature on top of the exponential decay to its asymptotic temperature. This can cause the temperature of two initial states to cross at finite time at strong system-bath couplings. This phenomenon is referred to as the Mpemba crossing. The Mpemba crossing describes a phenomenon that for different initial states the system observables, which are conventionally considered as state functions in a equilibrium setup, intersect at a finite time. The consequence of this crossing is that for

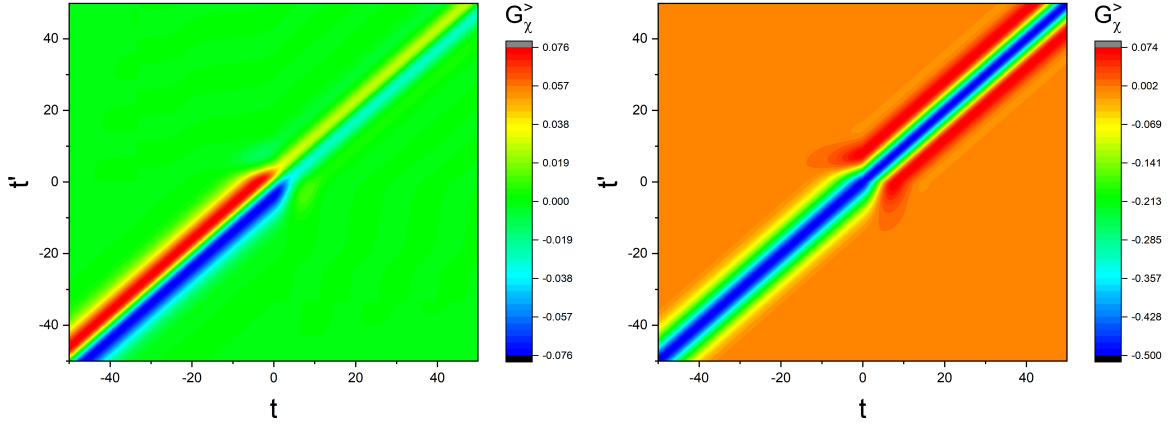


FIG. 5. The 2D map for the Green's function $G_\chi^>$. (a) The real component. (b) The imaginary component. The coupling between the system and the bath is set to be $V = 0.525$. The other parameters used in the numerical simulations are: $n = 3$, $J = 0.5$, $\beta_{\text{bath}} = 0.5$, $\beta_i = 2.4$, $\Delta t = 0.1$.

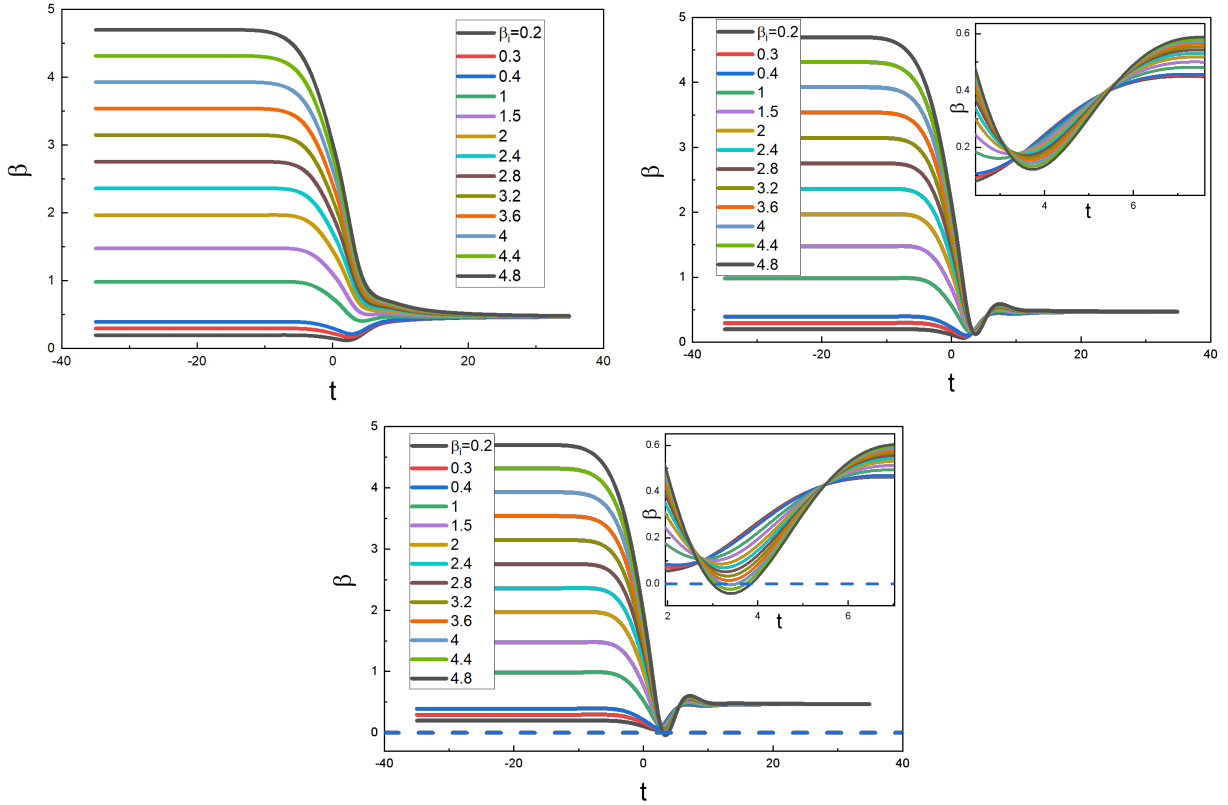


FIG. 6. The evolution of inverse temperature β vs time t . The coupling between the system and the bath is set to be (a) $V = 0.4$, (b) $V = 0.525$, and (c) $V = 0.55$. For weak system-bath couplings, the thermalization processes behave as expected. The anomalous effects only exist for strong couplings. For all, $n = 3$, $J = 0.5$, $\beta_{\text{bath}} = 0.5$.

an experimenter Alice who prepares two different systems immersed in the same thermal bath and constantly monitors an observable, for example, the effective temperature, Alice may find that the system with a higher initial temperature cools to a temperature lower than that of the system with a lower initial temperature at certain times during the continuous monitoring of the system temperatures. This is a reminiscence of the original Mpemba effect and falls into the current category of the general MPEs.

A solution to the KB equation for the Green's function $G_\chi^>(t, t')$ is shown in Fig. 5, where we have set the initial temperature of the system to be $\beta_i = 2.4$ and the temperature of the thermal bath to be $\beta_{\text{bath}} = 0.5$. As in the equilibrium situation, the Green's

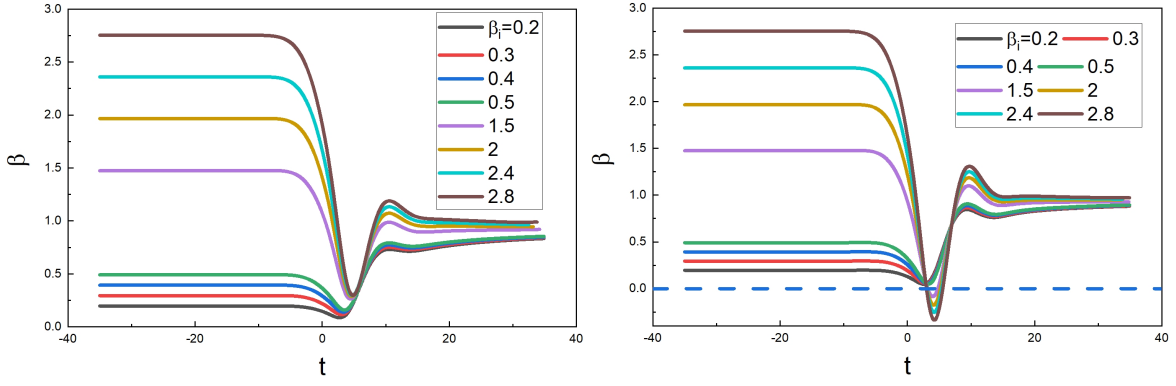


FIG. 7. MPCs and negative temperatures emerge at sufficiently strong couplings for $n = 1$ case. (a) The parameters are: $n = 1$, $V = 0.15$. (b) $n = 1$, $V = 0.175$. For both (a) and (b), $J = 0.5$, $\beta_{\text{bath}} = 0.5$.

function $G^>(t, t')$ decays rapidly away from the region near the diagonal slice $t = t'$. The system is coupled to the thermal bath at $t = 0$ and is in equilibrium before that. For strong system-bath couplings, the Green's function exhibits rapid variations near the $t, t' = 0$ and quickly relaxes to the steady state.

In Fig. 6 (a) and (b), we show that the Mpemba crossings only emerge when the coupling between the SYK system and the bath exceeds certain threshold value. For the weak couplings, the system's cooling dynamics resemble that of a quasi-equilibrium state so that our intuition from the equilibrium statistics works approximately in this situation. When the coupling is tuned up, the temperatures decay in the manner beyond the quasi-equilibrium description, the system with a lower (higher) initial temperature can be heated (cooled) to a temperature higher (lower) than the system starting from a higher (lower) initial temperature. The ‘‘Mpemba crossing’’ emerges as the result of the strong out-of-equilibrium of the system induced by the strong coupling between the bath and the system. The strong coupling can also induce anomalous phenomena similar to overheating and overcooling caused by the energy input into the system by the system-bath coupling and the collective oscillation of the system [see Fig. 14 in the Appendix]. The effective temperature can temporarily drops (rises) to a temperature lower (higher) than the asymptotic temperature in accordance with the ambient bath. In particular, when the coupling is sufficiently strong, the system is beyond the traditional equilibrium characterization and is accompanied by the emergence of negative temperatures according to the best fit of FDT [see Fig. 6(c)]. The negative temperature is usually considered as an indication that the system can dissipate heat to all equilibrium systems including those with $T = \infty$, which corresponds to the equal distribution of all energy levels. This appearance of the negative effective temperature is a distinct feature that the system is in strong nonequilibrium condition.

We remind that this oscillation of effective temperature is not necessarily just the redistribution of energy on different energy levels, the total energy can also manifest similar overheated phase due to the energy input induced by the strong coupling with the bath at $t = 0$. The total energy can be expressed as [37, 43]:

$$E(t) = \sum_{i_1 i_2 i_3 i_4} \frac{J_{i_1 i_2 i_3 i_4}}{4!} \overline{\langle \chi_{i_1} \chi_{i_2} \chi_{i_3} \chi_{i_4} \rangle} = \frac{iJ^2}{4} \int_{-\infty}^t dt' (G^>(t, t')^4 - G^<(t, t')^4). \quad (47)$$

An example of the dynamics of the total energy is shown in Fig. 14 in the Appendix. Interestingly, anomalous oscillations and an overheated phase also manifest during the relaxation processes in systems strongly coupled to thermal baths, especially when system's initial temperature is not significantly higher than the bath temperature. However, no MPCs are identified emerge in the dynamics of the total energy. This suggests that the temperature dynamics are the result of the contributions both from the total energy as well as the nonequilibrium statistics.

For the SYK model with $n = 1$, the oscillatory behavior after the quench is much more transparent than the $n = 3$ case as shown in Fig. 7. The effective temperature is driven up dramatically due to the energy input impulse when the coupling is turned on at $t = 0$ regardless of whether the bath temperature is higher or lower than the initial temperature of the SYK system. Another most noticeable feature from the simulation is that for $n = 1$ model, a lower coupling strength is required for the emergence of the Mpemba crossing as well as the negative temperature.

In summary, the quench dynamics of the SYK system coupled to a thermal bath reveal several anomalous behaviors, including oscillations in the effective temperature, temporal phases reminiscent of overheated and overcooled liquids, and Mpemba crossings between states that originate from different initial conditions. These observations hold true irrespective of the specific definition of the effective temperature. Results obtained using an alternative definition, Eq.(37), are presented in Fig. 13 in the Appendix. Though the MPEs in this system only appear shortly after the quench instead of in the asymptotic states as seen in simple integrable quantum systems such as the quantum-dot and quantum-spin systems, it nonetheless serves as a proof of principle for the existence of dynamical anomalies during thermalization in chaotic systems. Further investigation covering a

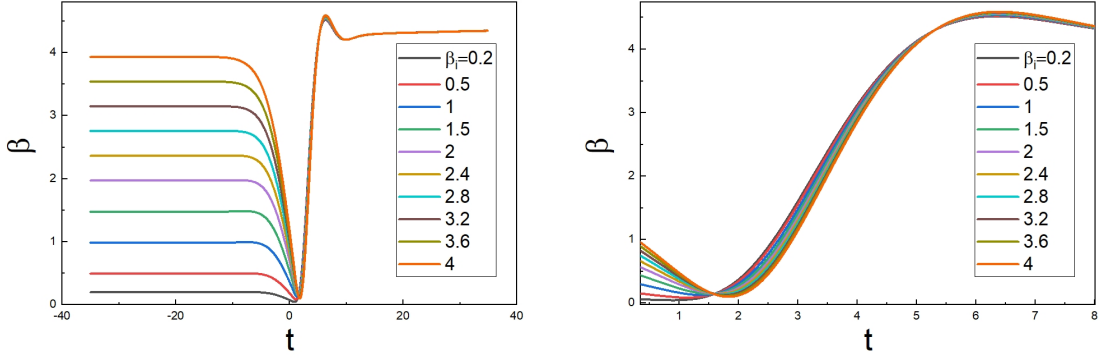


FIG. 8. Mpemba crossings in the case of two different baths. (a) The full dynamics from equilibrium states to the steady states. (b) A zoomed-in view of the dynamics. The parameters used in the numerical simulations are $n = 3$, $V_1 = V_2 = 0.5$, $\beta_{bath1} = 4.4$, $\beta_{bath2} = 4.8$.

broader parameter space and with additional model variations is likely to strengthen what is shown in this study.

IV. MPCs IN SYKS IN CONTACT WITH TWO DIFFERENT BATHS

The MPE is significantly more transparent and ubiquitous in systems simultaneously in contact with two different thermal baths in the quantum spin systems [11]. It was suggested that this is a result of the enhanced quantum coherence when the system is driven away from equilibrium [11, 56–58]. For N -level quantum spin systems described by the Lindblad equations, it is easy to identify the off-diagonal coherence terms sustained by the nonequilibrium conditions. However, whether such conclusions hold for the strongly-coupled SYK system is questionable. The SYK model coupled to a thermal bath, as described in the previous sections, can be easily generalized to the case with multiple baths. For example, we consider the SYK system simultaneously in contact with two thermal baths, the equations of motion is of the same KB form:

$$i\partial_{t_1} G_\chi^>(t_1, t_2) = \int dt_3 (\Sigma_\chi^R(t_1, t_3) G_\chi^>(t_3, t_2) + \Sigma_\chi^>(t_1, t_3) G_\chi^A(t_3, t_2)), \quad (48)$$

$$-i\partial_{t_2} G_\chi^>(t_1, t_2) = \int dt_3 (G_\chi^R(t_1, t_3) \Sigma_\chi^>(t_3, t_2) + G_\chi^>(t_1, t_3) \Sigma_\chi^A(t_3, t_2)), \quad (49)$$

while the corrections to the self-energy in Eq. (46) have extra contributions from both thermal baths:

$$\Sigma_\chi^>(t, t') = -J^2 (G_\chi^>(t, t'))^3 - V^2 (-1)^{\frac{n+1}{2}} \theta(t) \theta(t') (G_\psi^>(t, t'))^n - V'^2 (-1)^{\frac{n+1}{2}} \theta(t) \theta(t') (G_\psi^>(t, t'))^n, \quad (50)$$

$$\Sigma_\chi^<(t, t') = -J^2 (G_\chi^<(t, t'))^3 - V^2 (-1)^{\frac{n+1}{2}} \theta(t) \theta(t') (G_\psi^<(t, t'))^n - V'^2 (-1)^{\frac{n+1}{2}} \theta(t) \theta(t') (G_\psi^<(t, t'))^n, \quad (51)$$

$$\Sigma_\psi^<(t, t') = -J^2 (G_\psi^<(t, t'))^3, \quad (52)$$

$$\Sigma_\psi^>(t, t') = -J^2 (G_\psi^>(t, t'))^3. \quad (53)$$

Then, we follow the procedure introduced in the previous sections and numerically solve Eqs. (41) and (42) with the above self-energies. In contrast to the quantum dot system where MPE becomes more ubiquitous and emerges in less stringent criteria, in the open SYK system, larger coupling with the thermal bath is required to induce the Mpemba crossing. First of all, as shown in Fig. 8, the crossings of the different initial states start to emerge when the coupling is gradually tuned up. However, we notice that the crossings always occur $2N$ times, $N \in \mathbb{N}$, so that the MPE does not exist in the asymptotic final states, which requires $2N + 1$ crossings. In contrast with the conventional MPE where temperature changes are monotonic and state crossings emerge at most once, here the temperature dynamics are more complicated and the relative positions of the effective temperatures oscillate. In addition, different from the nonequilibrium MPEs in the integrable systems such as the quantum dot system and double-fermionic system, systems with larger biases between two bath temperatures require stronger bath-system couplings to necessitate the emergence of the MPCs [see Fig. 9]. Therefore, the temperature bias raises rather than lowers the threshold coupling, making it more difficult to observe the MPCs. This is another evidence that the MPCs in quantum integrable models have a different underlying mechanism from that in the SYK models. In Fig. 9], the mean temperature of the two baths

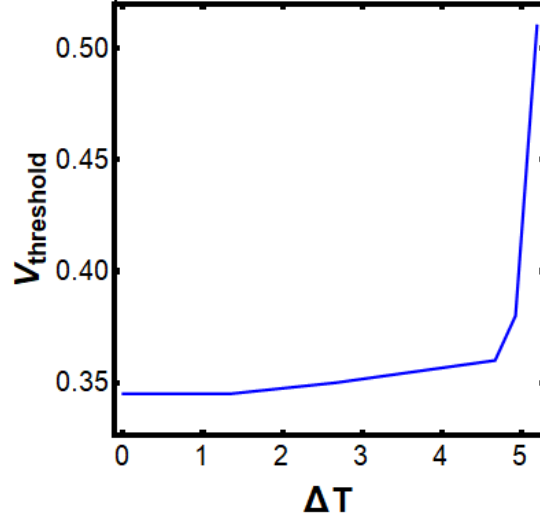


FIG. 9. The threshold coupling $V_{\text{threshold}}$ for the emergence of MPCs against the temperature bias between the two baths. The parameters used in the numerical simulations are: $n = 3$, $J = 0.5$, $\beta_{\text{bath}} = 0.5$.

are fixed at around $\bar{T} \approx 5.3J$ while we vary the temperature bias between them. Therefore, the nonequilibrium enhancement of the MPE, as discovered in Ref. [11], only emerges in the integrable models where the MPEs are induced by peculiarity of initial conditions and does not apply to the chaotic SYK systems where MPEs are induced by nonequilibrium.

V. DISAPPEARANCE OF MPCs IN LIOUVILLIAN SYK

Open SYK models can be modeled by the Lindblad master equations with linear jump operators. The Lindbladian SYK model is dual to the two-coupled SYK model where the real time t in the Lindbladian SYK model plays the role of the inverse temperature in double SYK model [32]. The common lore of the Lindblad equation is that the formalism gives a rough description of open systems while the very detailed information on the dynamics are erased. It is interesting to compare the quench dynamics derived from the SYK Lindbladian and that from the exact computation in the previous sections, and to find out whether the anomalies found in the previous sections can remain in this formalism. To compute the nonequilibrium Green's function, we employ the Schwinger-Keldysh formalism in the doubling Hilbert space with the vectorization of Liouvillian. In this way, the Lindblad equations of motion can be written in reminiscence of Schrödinger's equation and calculated from the Keldysh path integral.

A. Choi-Jamiolkowski isomorphism and Lindblad equation for SYK models

To simplify the formalism for computing the Green's functions of the dissipative SYK model, we map the density matrix to a vector in the double Hilbert space via the Choi-Jamiolkowski (CJ) isomorphism [59, 60], viz.,

$$\rho = \sum_{m,n} \rho_{m,n} |m\rangle\langle n| \quad \rightarrow \quad |\psi_{\rho}^D(t)\rangle = \sum_{m,n} \rho_{m,n} |m\rangle \otimes |n\rangle \in \mathcal{H}_L \otimes \mathcal{H}_R. \quad (54)$$

For states that satisfy the Lindblad equation:

$$\frac{d\rho}{dt} = -i[H, \rho] + 2\gamma \sum_m L_m \rho L_m^{\dagger} - \gamma \sum_m \{L_m^{\dagger} L_m, \rho\}, \quad (55)$$

the state vector can be viewed or rewritten as the “wavefunction” that satisfies the Schrödinger's equation:

$$i\partial_t \psi_{\rho}^D(t) = H^D \psi_{\rho}^D(t), \quad (56)$$

where $H^D = H_s - iH_d$ is defined on the double space, $H_s = H_L \otimes \mathbb{I}_R - \mathbb{I}_L \otimes H_R^T$, H_R^T is the transpose of H_R , $H_L = H_R = H$, and H_d is defined as follows:

$$H_d = \gamma \sum_m \left[-2L_m \otimes L_m^{\dagger T} + L^{\dagger} L_m \otimes \mathbb{I} + \mathbb{I} \otimes (L_m^{\dagger} L_m)^* \right]. \quad (57)$$

One can verify that the rule for a Lindbladian operator acting on the right Hilbert space (i.e., the operators to the right of the density matrix) is that it is simply changed to its transpose, viz., $L \rightarrow L^{\dagger*} = L^T$.

For the SYK model with the jump operators chosen to be $L_i = \sqrt{\mu}\psi_i$, the ground state of the Lindblad equation can be shown to be the maximally entangled state at the temperature $T = \infty$ [32, 38]. The goal is to find a representation of the transpose of the Majorana fermion operator ψ^T using ψ . One algorithm to find such representation is provided. The Majorana operators are elements of the Clifford algebra $Cl(N)$ represented by the gamma matrices $\psi_k = \gamma_k$. For the double-site Majorana operators, one can choose the following representation for simplicity:

$$\psi_L^k = \gamma_k \otimes \mathbb{I}, \quad \psi_R^k = \gamma_c \otimes \gamma_k, \quad (58)$$

where γ_c is the chiral matrix. We require that the transpose of the gamma matrix acting on the right Hilbert space is expressed as the right Majorana operator up to a constant and a global phase

$$\mathbb{I} \otimes \gamma_k^T \sum_j |j\rangle \otimes |j\rangle = \sum_j |j\rangle \otimes \gamma_k^T |j\rangle = \alpha (U \otimes U) \sum_j \gamma_c |j\rangle \otimes \gamma_k |j\rangle \quad (59)$$

for some constant α and matrix U . We can rewrite this equation as

$$\sum_j |j\rangle \gamma_k^T |j\rangle = \alpha \sum_j U \gamma_c |j\rangle U \gamma_k |j\rangle = \alpha \sum_j |j\rangle U \gamma_k \gamma_c^{-1} U^{-1} |j\rangle. \quad (60)$$

Then, we have

$$\gamma_k^T = \alpha \gamma_k \gamma_c^{-1} U^{-1}. \quad (61)$$

The equality of charge conjugation $C^{-1} \gamma_k C = \gamma_k^T$ gives

$$U = C^{-1} e^{\frac{i\pi}{4} \gamma_c}, \quad \alpha = -i. \quad (62)$$

Therefore, from the above derivation we have the representation of the transpose of the Majorana operator

$$\mathbb{I} \otimes \psi_k^T = -i \psi_R^k \quad (63)$$

With the above identification, one can write the Liouvillian operator in the doubled Hilbert space as

$$\mathcal{L} = -iH^D = -iH_L^{\text{SYK}} - i(-i)^q H_R^{\text{SYK}} - i\mu \sum_i \psi_L^i \psi_R^i - \frac{\mu N}{2} \quad (64)$$

where H^D is given in Eqs. (56) and (57). One can relate to the Keldysh formalism by introducing fields

$$\psi^i(t^+) = \psi_L(t) \quad \text{and} \quad \psi^i(t^-) = i\psi_R(t) \quad (65)$$

living on C^+ and C^- , respectively. The extra negative sign in $\psi^i(t^-) = i\psi_R(t)$ is due to the inverse time direction from $+\infty$ to $-\infty$ on the C^- branch of the contour. The Keldysh closed-time contour is $C = C^+ \cup C^-$. The Lindbladian SYK model in real time is dual to the Euclidean two-coupled SYK model by the following identifications [32]:

$$\begin{aligned} G_{LL} &\rightarrow -iG_{LL}, & G_{RR} &\rightarrow iG_{RR}, & G_{LR} &\rightarrow G_{LR}, & G_{RL} &\rightarrow G_{RL}, \\ \Sigma_{LL} &\rightarrow i\Sigma_{LL}, & \Sigma_{RR} &\rightarrow -i\Sigma_{RR}, & \Sigma_{LR} &\rightarrow -\Sigma_{LR}, & \Sigma_{RL} &\rightarrow i\Sigma_{RL}. \end{aligned} \quad (66)$$

B. SYK Lindbladian

Through Choi-Jamiolkowski isomorphism, the Lindbladian is mapped from the density matrix representation to the double-vector representation as follows [44, 61]:

$$\mathcal{L}(\rho) = -i[H_{\text{SYK}}, \rho] + \sum_{\alpha} \left[L_{\alpha} \rho L_{\alpha}^{\dagger} - \frac{1}{2} \{L_{\alpha}^{\dagger} L_{\alpha}, \rho\} \right] \rightarrow \mathcal{L} = -iH^D = -iH_L^{\text{SYK}} - i(-i)^q H_R^{\text{SYK}} - i\mu \sum_i \psi_L^i \psi_R^i - \frac{\mu N}{2} \quad (67)$$

where $L^i = \sqrt{\mu}\psi^i$ is the linear jump operator and H_{SYK} is given by

$$H_{L(R)}^{\text{SYK}}[J_{i_1 \dots i_q}, \psi] = \sum_{i_1 \dots i_q} \frac{J_{i_1 \dots i_q}}{4!} \psi_{i_1, L(R)} \dots \psi_{i_q, L(R)}. \quad (68)$$

The partition function is written as

$$Z = \int \mathcal{D}\psi_L \mathcal{D}\psi_R e^{iS[\mathcal{D}\psi_L, \mathcal{D}\psi_R]}, \quad (69)$$

where L, R live in the doubled Hilber space $\mathcal{H}_L \otimes \mathcal{H}_R$ and the action is given by

$$iS = \int_{-\infty}^{\infty} dt \left[-\frac{1}{2} \sum_i \psi_L^i \partial_t \psi_L^i - \frac{1}{2} \sum_i \psi_R^i \partial_t \psi_R^i + \mathcal{L} \right]. \quad (70)$$

We can left out the constant term in the vectorized Liouvillian, viz.,

$$\mathcal{L} = -iH^D = -iH_L^{\text{SYK}} - i(-i)^q H_R^{\text{SYK}} - i\mu \sum_i \psi_L^i \psi_R^i. \quad (71)$$

By introducing the Keldysh contour $C = C^+ \cup C^-$ and the fields $\psi(t^+) = \psi_L(t)$ with $t^+ \in C^+$, $\psi(t^-) = i\psi_R(t)$ with $t^- \in C^-$, one can rewrite the action as the following:

$$iS = - \int_C dz \frac{1}{2} \sum_i \psi^i(z) \partial_z \psi^i(z) - i \int_C dz i^{q/2} \sum_{i_1 < \dots < i_q} J_{i_1 \dots i_q} \psi^{i_1}(z) \dots \psi^{i_q}(z) + \mu \int_C dz dz' K(z, z') \sum_{i=1}^N \psi^i(z) \psi^i(z), \quad (72)$$

with the dissipation kernel

$$K(t_1^+, t_2^-) = \delta(t_1 - t_2), \quad K(t_1^+, t_2^+) = K(t_1^-, t_2^+) = K(t_1^-, t_2^-) = 0. \quad (73)$$

On the Keldysh contour, $dz = dt$ on C^+ and $dz = -dt$ on C^- . In terms of the collective variables (G, Σ) , where Σ is the Lagrange multiplier of G , the action reads

$$iS = \frac{N}{2} \{ \text{Tr} \log(i\partial_z - \Sigma) - \int_C dz dz' \Sigma(z, z') G(z, z') - \frac{i^q J^2}{q} \int_C dz dz' [G(z, z')]^q + 2i\mu \int_C dz dz' K(z, z') G(z, z') \}. \quad (74)$$

We apply the following identities that for an operator M :

$$\log(\det M) = \text{Tr} \log M, \quad \delta[\det M] = \det M \text{Tr}(M^{-1} \delta M), \quad (75)$$

and solve for the saddle point equation for the collective variables $\Sigma_{\alpha\beta}(t_1, t_2)$ and $G_{\alpha\beta}(t_1, t_2)$ by taking derivatives of the action with respect to $G_{\alpha\beta}(t_1, t_2)$ and $\Sigma_{\alpha\beta}(t_1, t_2)$, respectively. From the action, we can derive the saddle-point equations of motion for the Green's functions in the large- N limit, which are

$$(i\partial - \Sigma)G = \mathbf{1}_{\mathbb{C}}, \quad (76)$$

$$\Sigma_{\alpha\beta}(z, z') = -i^q J^2 G_{\alpha\beta}(z, z')^{q-1} + i\mu [K(z, z') - K(z', z)].$$

Restricting to the C^+ and C^- contours and switching to the integral equation, we have the KB equation as follows:

$$i\alpha \partial_{t_1} G_{\alpha\beta}(t_1, t_2) - \int dt_3 \sum_{\gamma=+,-} \Sigma_{\alpha\gamma}(t_1, t_3) G_{\gamma\beta}(t_3, t_2) = \delta_{\alpha\beta} \delta(t_1 - t_2), \quad (77)$$

$$\Sigma_{\alpha\beta}(t_1, t_2) = -i^q J^2 s_{\alpha\beta} G_{\alpha\beta}(t_1, t_2)^{q-1} + i\mu s_{\alpha\beta} \epsilon_{\alpha\beta} \delta(t_1 - t_2) \theta(t_1) \theta(t_2),$$

where $s_{++} = s_{--} = 1$, $s_{+-} = s_{-+} = -(-1)^{q/2}$, the Levi-Civita symbols are $\epsilon_{+-} = 1$, $\epsilon_{-+} = -1$, $\epsilon_{--} = \epsilon_{++} = 0$, and α/β are “ \pm ” signs. One can relate the lesser, time-ordered and anti-time-ordered Green's functions to the greater Green's function as follows:

$$G^<(t_1, t_2) = -G^>(t_2, t_1),$$

$$G^T(t_1, t_2) = G^{++}(t_1, t_2) = \theta(t_1 - t_2) G^>(t_1, t_2) + \theta(t_2 - t_1) G^<(t_1, t_2),$$

$$G^{\bar{T}}(t_1, t_2) = G^{--}(t_1, t_2) = \theta(t_2 - t_1) G^>(t_1, t_2) + \theta(t_1 - t_2) G^<(t_1, t_2). \quad (78)$$

Combining the Kadanoff-Baym equation (77) and the symmetry relation

$$G^>(t_1, t_2) = (G^<(t_1, t_2))^* = -(G^>(t_2, t_1))^* , \quad (79)$$

we numerically solve for the dynamics of the Green's functions. Note that for the $-+$ component of the Eq. (77), the upper limit of the integration only extends to $\max(t_1, t_2)$ and the integrand vanishes for $t_3 > \max(t_1, t_2)$.

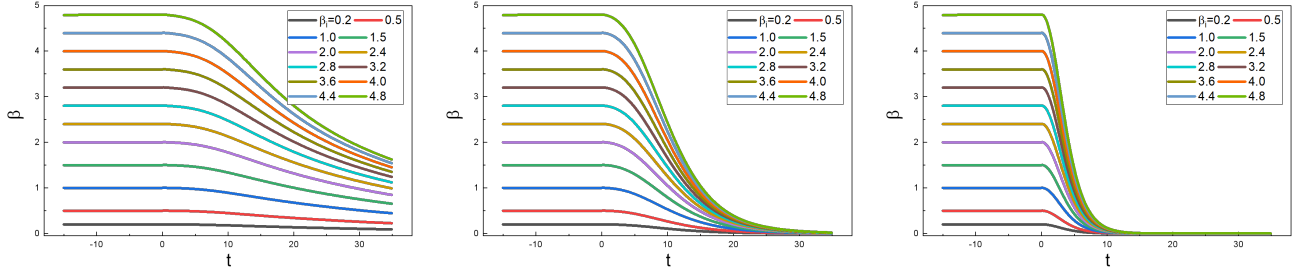


FIG. 10. The effective temperature dynamics in the Lindblad description at the dissipative constant (a) $\mu = 0.01$, (b) $\mu = 0.05$, (c) $\mu = 0.5$. The parameters used are $J = 0.5$, $q = 4$.

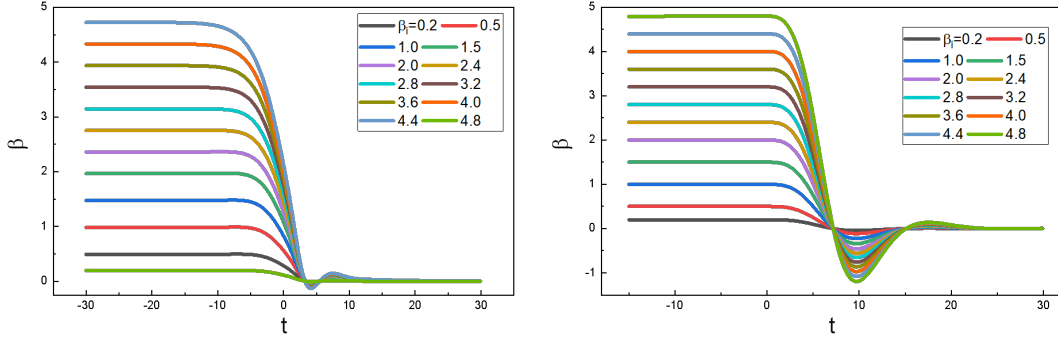


FIG. 11. The effective temperature dynamics in the exact calculation of SYKs coupled with baths at infinite temperature. (a) The dynamics of the effective temperature according to definition Eq. (34). (b) The dynamics of the effective temperature according to definition Eq. (37). The parameters used are $J = 0.5$, $q = 4$.

C. Numerical results and comparisons

To investigate quantum chaotic systems, we focus on SYK₄ in our numerical study. We vary the dissipative constant μ and the initial temperature of the system and numerically calculate the real-time dynamics of the SYKs dictated by the KB equation Eq. (103). The initial condition of the correlation functions can be derived from the correlators in the previous section, viz., for $t, t' < 0$:

$$G_l^{++}(t, t') = G_i^{++}(t, t'), \quad G_l^{+-}(t, t') = -iG_i^{+-}(t, t'), \quad (80)$$

$$G_l^{-+}(t, t') = -iG_i^{-+}(t, t'), \quad G_l^{--}(t, t') = -G_i^{--}(t, t'), \quad (81)$$

where G_i with subscript “i” denotes the corresponding correlator defined in Eq. (16). We set the system’s initial Green’s function $G_i^>(t, t') = G_i^{-+}(t, t')$ before the quench and then use the Eq. (103) to generate the dynamics of the system.

Interestingly, we did not find any anomalies in the dynamics of the effective temperature as those emerged in the exact solutions of the SYKs coupled with SYK baths. As shown in Fig. 10, the inverse of the effective temperature drops approximately exponentially at late times, corresponding to an exponential rise in temperature. The dynamics share resemblance with that in quasi-equilibrium approximation where the inverse temperature decreases smoothly and monotonically after $t = 0$ with trajectories from different initial states well-separated before converging to the steady state. In contrast to the Lindbladian dynamics, we can also compute the inverse temperature dynamics by coupling the SYK model to an infinite-temperature SYK bath. The results are shown in Fig. 11, where we identify similar collective oscillations of the system temperatures and MPCs in the heating process.

The two sets of numerical results show a clear difference between direct solving the KB equations with infinite-temperature thermal baths and solving the SYK Lindblad equation. It is worth mentioning that the two SYK models do not relax to the same equilibrium state, even though both final states have inverse temperature zero. One way to understand such distinction is by noticing that the KB equation of the Lindbladian SYK can be related to the KB equation of an SYK system coupled to a thermal bath by substituting the bath’s time correlation in the self energies with one proportional to a Dirac delta function in time, i.e., $i\delta(t - t')$ as in Eq. (77). In many weakly interacting quantum systems, the vanishing width of the Green’s function typically corresponds to the system reaching an infinite temperature. However, the SYK model has nontrivial real-time dynamics

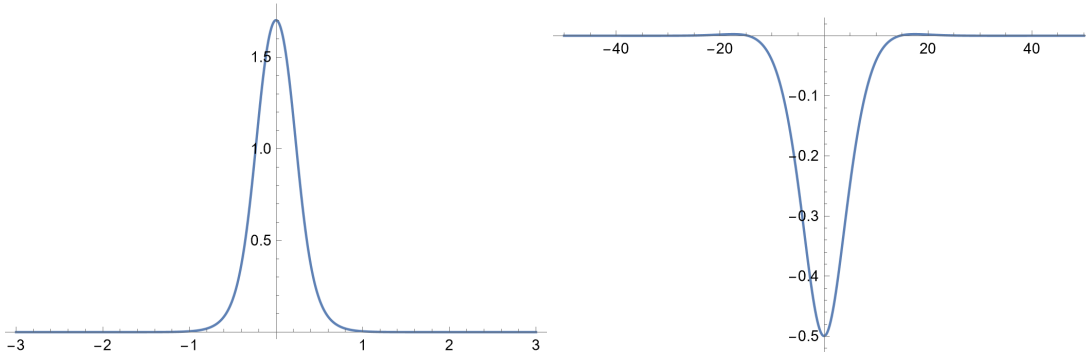


FIG. 12. The imaginary part of the Green's function at infinite temperature from solving the self-consistency equation Eq. (30). (a) The spectrum of the Green's function $\text{Im}(G(\omega))$ at $\beta \rightarrow 0$. (b) $\text{Im}(G(t))$ at $\beta \rightarrow 0$. For a finite SYK coupling J , the imaginary part of the correlation function does not return to the delta function. The imaginary part of the correlation function returns to the delta function only in the strongly-coupled limit.

even at the temperature $T = \infty$ and the spectral function remains approximately the unchanged beyond a certain temperature threshold. The fact that the SKY Green's function has finite width proportional to the SYK coupling was also pointed out in Ref. [62], where it was argued that the quasi-particle decay rate satisfies $\Gamma \approx \frac{1}{\sqrt{q-12q/2-2}}J$ assuming the form of Green's function $G^R(\omega) \approx \frac{1}{\omega+i\Gamma}$. This difference in the spectrum causes a clear distinction of the Lindbladian SYK model from a dissipative SYK model in a thermal bath.

To recapitulate, we find that the Lindbladian SYK approach, though mimicking SYK model in an infinite-temperature bath, does not admit the same MPCs as in the SYK models coupled to thermal baths at $\beta = 0$. The results show that the common lore about the Lindblad equations—averaging over fast modes and suppressing quantum oscillations in the system—effectively remains valid in this context. One of the reasons for the difference is that SYK models still have nontrivial real-time dynamics at $T = \infty$ and finite widths in its imaginary part of the two-point function, contrasting the flat spectrum across all frequencies of the delta function in the Lindblad equation.

VI. DISCUSSION AND CONCLUSION

Though only manifest part of the most salient features of the MPE, the SYK models share crucial similarities with the original MPE in the thermalization process. The temperature crossings observed in these chaotic systems are not merely a quantum analogy appearing to have an eye-catching outfit of an MPE, they stem from the same underlying mechanism: the strongly nonequilibrium dynamics that drive the system statistics away from quasi-equilibrium approximations. In contrast, in many simple quantum models (e.g., quantum dot or qudit models), the origins of the MPEs can be attributed to factors like the specialty of initial conditions and the properties of the chosen observables (e.g., entanglement asymmetry and trace distance, et al.). None of these properties are pertinent to the core of classical MPEs: the strongly nonequilibrium dynamics. For classical systems cooled at an extremely slow rate, quasi-equilibrium analysis still applies and no MPE appears. Similarly, the MPEs in the SYK models appear only when the system-bath couplings exceed certain threshold so that the strong interactions rapidly drive the systems far from any equilibrium states. Such effects do not require the fine tuning of initial conditions. The above distinction allows us to categorize MPCs into the nonequilibrium driven and the initial condition driven.

Some may argue that the temperature crossing could be due to the ill-defined nature of temperatures in nonequilibrium settings. It is crucial to note that even in the classical Mpemba system, the temperature evolution during the cooling process should be understood as a measurement of effective temperature, which only reflects certain statistical properties rather than the full microscopic state of the system. This is especially true when the system is rapidly cooled, a condition that facilitates the emergence of MPE. In the classical nonequilibrium systems, the energy distribution and dynamics often differ from those in thermal equilibrium (exemplified by the presence of macroscopic flows or turbulence) even when their effective temperatures are identical. In the large- N limit of SYK systems, the emergence of Mpemba crossings (MPCs) is similarly related to the limited information the effective temperature can capture. While the concept of temperature is only uniquely-defined for systems in equilibrium, one can always measure the (effective) temperature of a system using a thermometer regardless of the equilibrium condition. The effective temperature serves as a useful experimental observable and coincides with the temperature when the measured system is close to equilibrium. Besides, our conclusions are unchanged for different characterizations of temperature. For both classical and SYK systems, the core mechanism behind the MPEs is the same—the effective temperature does not fully describe the underlying microscopic states and the full nonequilibrium behaviors of the system—so that different initial states

do not repeat the same state paths even when their temperatures coincide. The SYK systems, when strongly interacting with baths, push this phenomenon to its extreme, showcasing how deviations from equilibrium can drive the MPE. This observation is consistent with existing research on the classical MPE, where rapid cooling and nonequilibrium conditions lead to unexpected temperature evolution. In the quantum context, studies of SYK and related models have shown that strong interactions with the baths introduce similar anomalies, exhibiting a universality of the general MPE across different physical systems.

Generally, the existence of the MPCs in quantum systems is very dependent on which observables one chooses to measure. Though tracking the system temperatures bears more resemblance to the classical MPE, concepts such as entanglement entropy and Loschmidt amplitude, which are well-defined regardless of the equilibrium condition, are also interesting to study. While the MPCs in SYK models provide valuable insights into nonequilibrium dynamics, their emergence in black hole quench dynamics remains an open question. Given that the low energy dynamics of a SYK model are dual to the JT gravity, the emergence of MPCs in dissipative SYK models may indicate similar phenomena in the nonequilibrium quench dynamics of black holes in thermal baths. However, this may require strong couplings between the external baths and the black holes and it is not completely clear if the duality can be extended to that regime. The study is far from being conclusive in this perspective and further investigation in the black hole quench dynamics is needed to consolidate the above indication.

In conclusion, the emergence of the nonequilibrium-driven MPCs is a showcase of a new distinctive feature of strongly nonequilibrium systems which is absent in close-to-equilibrium systems, contrasting the initial-condition-driven MPCs. We show that this effect can emerge in chaotic systems with large degrees of freedom, which bear resemblance to the JT gravity, and that the underlying mechanism for its emergence differs from that in the integrable quantum systems. As demonstrated in the Lindbladian SYK dynamics, the emergence of the MPEs is also dependent on the way the system is driven besides the coupling strength. In addition, the nonequilibrium conditions of the bath, which facilitate the MPE in quantum dot systems, elevate the threshold for its emergence. The results from this study on chaotic systems, combined with previous studies on integrable systems, suggest that Mpemba-like effects are likely ubiquitous across a wide range of strongly nonequilibrium systems, potentially including black holes.

ACKNOWLEDGEMENT

X.W. wants to thank Tokiro Numasawa and Huajia Wang for helpful discussions, and thank Pengfei Zhang for discussions, assistance in numerical simulations and feedback on the initial draft of the paper. X.W. also acknowledges the hospitality of Kavli Institute of Theoretical Sciences, University of Chinese Academy of Sciences and the workshop Holography in Beijing 2024 at KITS where some content of the paper was discussed.

AUTHOR CONTRIBUTION

X.W. designed the research and performed the analytical calculations. J.S. and X.W. conducted the numerical simulations. X.W., J.S., and J.W. contributed to discussions, as well as the shaping and writing of the manuscript. The authors declare no conflict of interest.

APPENDIX

A. Definitions and equations for numerical simulations

The dynamics of the SYK system after the quench can be described by the Kadanoff-Baym equations, the equations of motion of the system. In these equations, the influence of the bath on the SYK model is of order one, while the influence of the SYK model on the self energy of the bath is of higher orders in the large- N expansion and can be ignored. The Kadanoff-Baym equation is solved numerically. For the SYK systems in the thermal bath, we need to solve for $G_\chi^>(t, t')$ and $G_\chi^<(t, t')$. For $t, t' < 0$, the Green's functions are known from the computed data of the SYK system in thermal equilibrium, viz., $G_\chi^>(t, t') = G_\chi^>(t - t')$, where we have assumed the translational invariance. The data can be easily discretized and stored in terms of $\{\Delta t, G_\chi^>(\Delta t)\}$ for numerical simulation using trapezoidal method.

$$\Sigma_R(t, t') = \theta(t - t')(\Sigma^>(t, t') - \Sigma^<(t, t')), \quad (82)$$

$$\Sigma_A(t, t') = \theta(t' - t)(\Sigma^<(t, t') - \Sigma^>(t, t')), \quad (83)$$

$$\Sigma_K(t, t') = \Sigma^<(t, t') + \Sigma^>(t, t'). \quad (84)$$

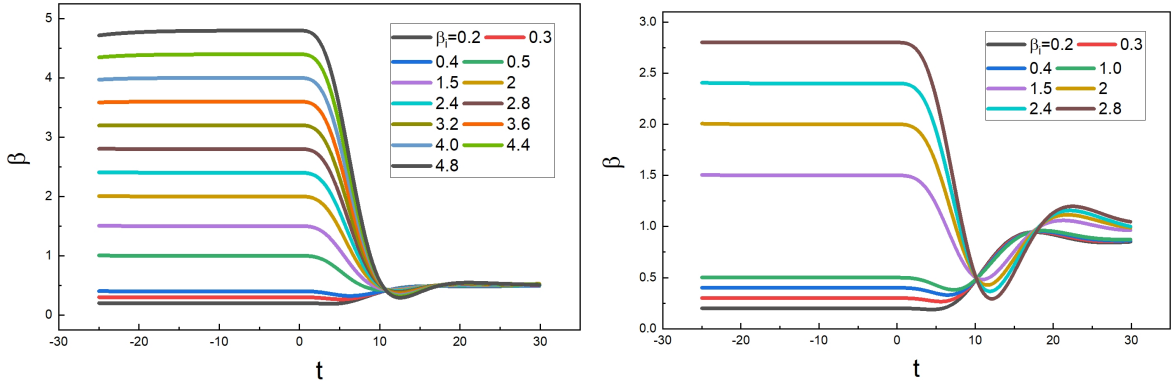


FIG. 13. Dynamics of the inverse effective temperature according to Eq. (37). (a) $n = 3$, $\beta = 0.5$, $V = 0.4$, $J = 0.5$. (b) $n = 1$, $\beta = 1.0$, $V = 0.15$, $J = 0.5$.

$$G_{\chi}^{\gt}(t, t') = (G_{\chi}^{\lt}(t, t'))^*, \quad (85)$$

$$G_{\psi}^{\gt}(t, t') = (G_{\psi}^{\lt}(t, t'))^*, \quad (86)$$

$$\Sigma_{\chi}^R(t, t') = \theta(t - t')(\Sigma_{\chi}^{\gt}(t, t') - \Sigma_{\chi}^{\lt}(t, t')), \quad (87)$$

$$\Sigma_{\chi}^A(t, t') = \theta(t' - t)(\Sigma_{\chi}^{\lt}(t, t') - \Sigma_{\chi}^{\gt}(t, t')), \quad (88)$$

$$G_{\chi}^A(t, t') = \theta(t' - t)(G_{\chi}^{\lt}(t, t') - G_{\chi}^{\gt}(t, t')), \quad (89)$$

$$G_{\chi}^R(t, t') = \theta(t - t')(G_{\chi}^{\gt}(t, t') - G_{\chi}^{\lt}(t, t')) \quad (90)$$

$$\Sigma_{\chi}^{\gt}(t, t') = -J^2(G_{\chi}^{\gt}(t, t'))^3 - V^2(-1)^{\frac{n+1}{2}}\theta(t)\theta(t')(G_{\psi}^{\gt}(t, t'))^n, \quad (91)$$

$$\Sigma_{\chi}^{\lt}(t, t') = -J^2(G_{\chi}^{\lt}(t, t'))^3 - V^2(-1)^{\frac{n+1}{2}}\theta(t)\theta(t')(G_{\psi}^{\lt}(t, t'))^n, \quad (92)$$

$$\Sigma_{\psi}^{\lt}(t, t') = -J^2(G_{\psi}^{\lt}(t, t'))^3, \quad (93)$$

$$\Sigma_{\psi}^{\gt}(t, t') = -J^2(G_{\psi}^{\gt}(t, t'))^3. \quad (94)$$

$$i\partial_{t_1} G_{\chi}^{\gt}(t_1, t_2) = \int dt_3 (\Sigma_{\chi}^R(t_1, t_3)G_{\chi}^{\gt}(t_3, t_2) + \Sigma_{\chi}^{\gt}(t_1, t_3)G_{\chi}^A(t_3, t_2)), \quad (95)$$

$$-i\partial_{t_2} G_{\chi}^{\gt}(t_1, t_2) = \int dt_3 (G_{\chi}^R(t_1, t_3)\Sigma_{\chi}^{\gt}(t_3, t_2) + G_{\chi}^{\gt}(t_1, t_3)\Sigma_{\chi}^A(t_3, t_2)). \quad (96)$$

B. A different convention used for Liouvillian SYK model

In this section, we provide a different set of definitions and the corresponding KB equations frequently used for the dissipative SYK model [33, 61]. The Green's functions are related as follows:

$$G_{\alpha\beta}(t, t') = -i\langle \psi_{\alpha}(t)\psi_{\beta}(t') \rangle = \begin{pmatrix} G^{++}(t, t') & G^{+-}(t, t') \\ G^{-+}(t, t') & G^{--}(t, t') \end{pmatrix} = \begin{pmatrix} G^T(t, t') & G^{\lt}(t, t') \\ G^{\gt}(t, t') & G^{\bar{T}}(t, t') \end{pmatrix}, \quad (97)$$

where $\alpha, \beta = \pm$, and $G^T(t, t')$ and $G^{\bar{T}}(t, t')$ are defined as follows:

$$G^T(t, t') = G^{++}(t, t') = i(\theta(t - t')G^{\gt}(t, t') + \theta(t' - t)G^{\lt}(t, t')), \quad (98)$$

$$G^{\bar{T}}(t, t') = G^{--}(t, t') = -i(\theta(t' - t)G^{\gt}(t, t') + \theta(t - t')G^{\lt}(t, t')). \quad (99)$$

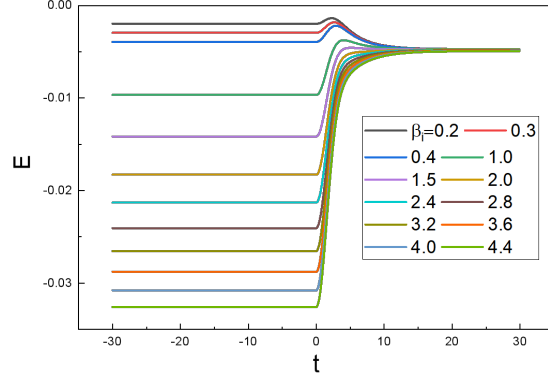


FIG. 14. The time evolution of the total energy of the SYK model coupled with a bath. The parameters used are $n = 3$, $\beta = 0.5$, $V = 0.525$, $J = 0.5$.

From the Lagrangian Eq. (70), which is

$$iS = \int_{-\infty}^{\infty} dt - \frac{1}{2} \sum_i \psi_+^i \partial_t \psi_+^i - \frac{1}{2} \sum_i \psi_-^i \partial_t \psi_-^i - i^{q+1} \sum_{i_1 < \dots < i_q} J_{i_1 \dots i_q} \psi_+^{i_1} \dots \psi_+^{i_q} + i^{q+1} \sum_{i_1 < \dots < i_q} J_{i_1 \dots i_q} \psi_-^{i_1} \dots \psi_-^{i_q} - i\mu \sum_i \psi_+^i(t) \psi_-^i(t), \quad (100)$$

where we have left out the constant term proportional to μN . This action can be studied as the ordinary SYK in the large N with the introduction of the collective fields Σ and G . The action of the vectorized Lindblad equation in terms of the collective variables reads:

$$S[G, \Sigma] = -\frac{iN}{2} \ln \det[-i(G_0^{-1} - \Sigma)] + \frac{i^{q+1} J^2 N}{2q} \int_{t_1}^{t_2} dt_1 dt_2 \sum_{\alpha, \beta} s_{\alpha, \beta} G_{\alpha, \beta}(t_1, t_2)^q + \frac{iN}{2} \int_{t_1}^{t_2} dt_1 dt_2 \sum_{\alpha, \beta} \Sigma_{\alpha, \beta}(t_1, t_2) G_{\alpha, \beta}(t_1, t_2) - \frac{i\mu N}{2} \int_{t_1}^{t_2} dt [G_{+-}(t, t) - G_{-+}(t, t)]. \quad (101)$$

We apply the following identities that for an operator M ,

$$\log(\det M) = \text{Tr} \log M, \quad \delta[\det M] = \det M \text{Tr}(M^{-1} \delta M), \quad (102)$$

and solve for the saddle point equation for the collective variables $\Sigma_{\alpha, \beta}(t_1, t_2)$ and $G_{\alpha, \beta}(t_1, t_2)$ by taking derivatives of the action with respect to $G_{\alpha, \beta}(t_1, t_2)$ and $\Sigma_{\alpha, \beta}(t_1, t_2)$, respectively. Then, we obtain the Kadanoff-Baym equation for the dissipative SYK model, which is

$$i\partial_{t_1} G_{\alpha\beta}(t_1, t_2) - \int dt_3 \sum_{\gamma=+,-} \Sigma_{\alpha\gamma}(t_1, t_3) G_{\gamma\beta}(t_3, t_2) = \delta_{\alpha\beta} \delta(t_1 - t_2), \quad (103)$$

$$\Sigma_{\alpha\beta}(t_1, t_2) = -i^q J^2 s_{\alpha\beta} G_{\alpha\beta}(t_1, t_2)^{q-1} + \theta(t_1) \theta(t_2) \mu \epsilon_{\alpha\beta} \delta(t_1 - t_2).$$

Here $s_{++} = s_{--} = 1$, $s_{+-} = s_{-+} = -(-1)^{q/2}$ and $\epsilon_{\alpha\beta}$ is the Levi-Civita symbol defined as $\epsilon_{+-} = 1$, $\epsilon_{-+} = -1$, $\epsilon_{--} = \epsilon_{++} = 0$. The time derivative with respect to t_2 can be obtained by the symmetry relation $\partial_{t_2} G^>(t_1, t_2) = (\partial_{t_2} G^>(t_2, t_1))^*$ or $\partial_{t_2} G^>(t_1, t_2) = -\partial_{t_2} G^<(t_2, t_1)$. For Majorana fermions, the differential equation with respect to t_1 suffices for solving the Wightman Green's function due to the symmetry of Green's function given by

$$G^>(t_1, t_2) = -(G^<(t_1, t_2))^* = (G^>(t_2, t_1))^*, \quad \text{or} \quad G^>(t_1, t_2) = -G^<(t_2, t_1). \quad (104)$$

Notice the sign difference from the two-coupled SYK models.

It is important to note the difference between the above definition and the notation used in the SYK systems coupling with a bath, especially when carrying out numerical simulations. In the above Liouvillian setup, the initial condition can be set to the thermal state at the inverse temperature β . The Green's functions of the initial thermal state in this formalism is related to the Green's function in the isolated SYK model by the following identifications: $G_l^{>>}(t, t') = G_i^{>>}(t, t')$, $G_l^{>-}(t, t') = -iG_i^{>-}(t, t')$,

$G_i^{-+}(t, t') = -iG_i^{+-}(t, t')$, and $G_i^{--}(t, t') = -G_i^{++}(t, t')$, where $G_i^{\alpha\beta}$ is the Green's function in the Liouvillian SYK and $G_i^{\alpha\beta}$ is the Green's function for an isolated SYK model. In this setup, the effective temperature can be defined through FDT as:

$$\beta(t) = \frac{2 \cdot \text{Re}(G_K(\omega, t))}{\omega \cdot \text{Re}(G_R(\omega, t))} \Big|_{\omega \rightarrow 0}. \quad (105)$$

-
- [1] M. Jeng, The mpemba effect: When can hot water freeze faster than cold?, *American Journal of Physics* **74**, 514 (2006).
- [2] A. Lasanta, F. V. Reyes, A. Prados, and A. Santos, When the hotter cools more quickly: Mpemba effect in granular fluids, *Physical review letters* **119**, 148001 (2017).
- [3] A. Biswas, V. Prasad, O. Raz, and R. Rajesh, Mpemba effect in driven granular maxwell gases, *Physical Review E* **102**, 012906 (2020).
- [4] A. Megías, A. Santos, and A. Prados, Thermal versus entropic mpemba effect in molecular gases with nonlinear drag, *Physical Review E* **105**, 054140 (2022).
- [5] A. Santos and A. Prados, Mpemba effect in molecular gases under nonlinear drag, *Physics of Fluids* **32** (2020).
- [6] S. A. Shapira, Y. Shapira, J. Markov, G. Teza, N. Akerman, O. Raz, and R. Ozeri, The mpemba effect demonstrated on a single trapped ion qubit, arXiv preprint arXiv:2401.05830 (2024).
- [7] L. K. Joshi, J. Franke, A. Rath, F. Ares, S. Murciano, F. Kranzl, R. Blatt, P. Zoller, B. Vermersch, P. Calabrese, *et al.*, Observing the quantum mpemba effect in quantum simulations, arXiv preprint arXiv:2401.04270 (2024).
- [8] Z. Lu and O. Raz, Nonequilibrium thermodynamics of the markovian mpemba effect and its inverse, *Proceedings of the National Academy of Sciences* **114**, 5083 (2017).
- [9] K. Chalas, F. Ares, C. Rylands, and P. Calabrese, Multiple crossing during dynamical symmetry restoration and implications for the quantum mpemba effect, arXiv preprint arXiv:2405.04436 (2024).
- [10] I. Klich, O. Raz, O. Hirschberg, and M. Vucelja, Mpemba index and anomalous relaxation, *Physical Review X* **9**, 021060 (2019).
- [11] X. Wang and J. Wang, Mpemba effects in nonequilibrium open quantum systems, *Phys. Rev. Res.* **6**, 033330 (2024).
- [12] H. C. Burrridge and P. F. Linden, Questioning the mpemba effect: hot water does not cool more quickly than cold, *Scientific Reports* **6**, 1 (2016).
- [13] J. Jin and W. A. Goddard III, Mechanisms underlying the mpemba effect in water from molecular dynamics simulations, *The Journal of Physical Chemistry C* **119**, 2622 (2015).
- [14] M. Moroder, O. Culhane, K. Zawadzki, and J. Goold, Thermodynamics of the quantum mpemba effect, *Phys. Rev. Lett.* **133**, 140404 (2024).
- [15] C. Rylands, K. Klobas, F. Ares, P. Calabrese, S. Murciano, and B. Bertini, Microscopic origin of the quantum mpemba effect in integrable systems, *Physical Review Letters* **133**, 010401 (2024).
- [16] A. K. Chatterjee, S. Takada, and H. Hayakawa, Quantum mpemba effect in a quantum dot with reservoirs, *Physical Review Letters* **131**, 080402 (2023).
- [17] F. Carollo, A. Lasanta, and I. Lesanovsky, Exponentially accelerated approach to stationarity in markovian open quantum systems through the mpemba effect, *Physical Review Letters* **127**, 060401 (2021).
- [18] S. Murciano, F. Ares, I. Klich, and P. Calabrese, Entanglement asymmetry and quantum mpemba effect in the xy spin chain, *Journal of Statistical Mechanics: Theory and Experiment* **2024**, 013103 (2024).
- [19] S. Yamashika, F. Ares, and P. Calabrese, Entanglement asymmetry and quantum mpemba effect in two-dimensional free-fermion systems, *Physical Review B* **110**, 085126 (2024).
- [20] S. Liu, H.-K. Zhang, S. Yin, and S.-X. Zhang, Symmetry restoration and quantum mpemba effect in symmetric random circuits, arXiv preprint arXiv:2403.08459 (2024).
- [21] A. K. Chatterjee, S. Takada, and H. Hayakawa, Multiple quantum mpemba effect: exceptional points and oscillations, *Physical Review A* **110**, 022213 (2024).
- [22] J. Maldacena, S. H. Shenker, and D. Stanford, A bound on chaos, *Journal of High Energy Physics* **2016**, 1 (2016).
- [23] A. Touil and S. Deffner, Information scrambling versus decoherence—two competing sinks for entropy, *PRX Quantum* **2**, 010306 (2021).
- [24] T. Scaffidi and E. Altman, Chaos in a classical limit of the sachdev-ye-kitaev model, *Physical Review B* **100**, 155128 (2019).
- [25] G. Casati and T. Prosen, Quantum chaos, in *Statistical and Nonlinear Physics* (Springer, 2022) pp. 561–573.
- [26] J. Maldacena and D. Stanford, Remarks on the sachdev-ye-kitaev model, *Physical Review D* **94**, 106002 (2016).
- [27] Y. Gu, X.-L. Qi, and D. Stanford, Local criticality, diffusion and chaos in generalized sachdev-ye-kitaev models, *Journal of High Energy Physics* **2017**, 1 (2017).
- [28] S. Sachdev and J. Ye, Gapless spin-fluid ground state in a random quantum heisenberg magnet, *Physical review letters* **70**, 3339 (1993).
- [29] A. Kitaev, A simple model of quantum holography, Talks at KITP strings seminar and Entanglement 2015 program <http://online.kitp.ucsb.edu/online/entangled15> (Feb. 12, April 7, and May 27, 2015).
- [30] J. Polchinski and V. Rosenhaus, The spectrum in the sachdev-ye-kitaev model, *Journal of High Energy Physics* **2016**, 1 (2016).
- [31] S. H. Shenker and D. Stanford, Multiple shocks, *Journal of High Energy Physics* **2014**, 1 (2014).
- [32] A. M. García-García, L. Sá, J. J. Verbaarschot, J. P. Zheng, *et al.*, Keldysh wormholes and anomalous relaxation in the dissipative sachdev-ye-kitaev model, *Physical Review D* **107**, 106006 (2023).
- [33] K. Kawabata, A. Kulkarni, J. Li, T. Numasawa, and S. Ryu, Dynamical quantum phase transitions in sachdev-ye-kitaev lindbladans, *Physical Review B* **108**, 075110 (2023).
- [34] A. M. García-García and V. Godet, Euclidean wormhole in the sachdev-ye-kitaev model, *Physical Review D* **103**, 046014 (2021).

- [35] A. M. García-García, Y. Jia, D. Rosa, and J. J. Verbaarschot, Dominance of replica off-diagonal configurations and phase transitions in a pt symmetric sachdev-ye-kitaev model, *Physical Review Letters* **128**, 081601 (2022).
- [36] Y. Chen, H. Zhai, and P. Zhang, Tunable quantum chaos in the sachdev-ye-kitaev model coupled to a thermal bath, *Journal of High Energy Physics* **2017**, 1 (2017).
- [37] P. Zhang, Evaporation dynamics of the sachdev-ye-kitaev model, *Physical Review B* **100**, 245104 (2019).
- [38] C. Zanoci and B. Swingle, Energy transport in sachdev-ye-kitaev networks coupled to thermal baths, *Physical review research* **4**, 023001 (2022).
- [39] A. Eberlein, V. Kasper, S. Sachdev, and J. Steinberg, Quantum quench of the sachdev-ye-kitaev model, *Physical Review B* **96**, 205123 (2017).
- [40] A. Almheiri, A. Milekhin, and B. Swingle, Universal constraints on energy flow and syk thermalization, *Journal of High Energy Physics* **2024**, 1 (2024).
- [41] J. Maldacena and A. Milekhin, Syk wormhole formation in real time, *Journal of High Energy Physics* **2021**, 1 (2021).
- [42] Y. Cheipesh, A. Pavlov, V. Ohanesjan, K. Schalm, and N. Gnezdilov, Quantum tunneling dynamics in a complex-valued sachdev-ye-kitaev model quench-coupled to a cool bath, *Physical Review B* **104**, 115134 (2021).
- [43] R. Bhattacharya, D. P. Jatkar, and N. Sorokhaibam, Quantum quenches and thermalization in syk models, *Journal of High Energy Physics* **2019**, 1 (2019).
- [44] L. Sá, P. Ribeiro, and T. Prosen, Lindbladian dissipation of strongly-correlated quantum matter, *Physical Review Research* **4**, L022068 (2022).
- [45] H. Wang, C. Liu, P. Zhang, and A. M. García-García, Entanglement transition and replica wormholes in the dissipative sachdev-ye-kitaev model, *Physical Review D* **109**, 046005 (2024).
- [46] A. M. García-García, J. J. Verbaarschot, and J.-p. Zheng, Lyapunov exponent as a signature of dissipative many-body quantum chaos, *Physical Review D* **110**, 086010 (2024).
- [47] F. Ares, S. Murciano, and P. Calabrese, Entanglement asymmetry as a probe of symmetry breaking, *Nature Communications* **14**, 2036 (2023).
- [48] A. Nava and R. Egger, Mpemba effects in open nonequilibrium quantum systems, *Physical Review Letters* **133**, 136302 (2024).
- [49] M. Babadi, E. Demler, and M. Knap, Far-from-equilibrium field theory of many-body quantum spin systems: Prethermalization and relaxation of spin spiral states in three dimensions, *Physical Review X* **5**, 041005 (2015).
- [50] A. Kamenev, *Field theory of non-equilibrium systems* (Cambridge University Press, 2023).
- [51] R. Kubo, The fluctuation-dissipation theorem, *Reports on progress in physics* **29**, 255 (1966).
- [52] Z. Zhang, X. Wang, and J. Wang, Quantum fluctuation-dissipation theorem far from equilibrium, *Physical Review B* **104**, 085439 (2021).
- [53] Here, we make a small comment about the different conventions as pointed out by Pengfei Zhang. The effective temperature are sometimes written as [37]

$$\beta(t) = 2 \frac{d}{d\omega} \left(\frac{G_{\chi,K}(\omega, t)}{G_{\chi,R}(\omega, t) - G_{\chi,A}(\omega, t)} \right)_{\omega=0}. \quad (106)$$

In this convention, we remind that the Wigner transformation

$$G(\omega, t) = \int_{-\infty}^{\infty} dt' e^{i\omega t'} G(t + t'/2, t - t'/2) \quad (107)$$

has different integration limits from Eq. (33).

- [54] This is also pointed out in Ref. [40].
- [55] Note that the difference between this equation and Eq. (34) is due to the different convention used in the fluctuation-dissipation relation.
- [56] X. Wang and J. Wang, Nonequilibrium effects on quantum correlations: Discord, mutual information, and entanglement of a two-fermionic system in bosonic and fermionic environments, *Physical Review A* **100**, 052331 (2019).
- [57] X. Wang and J. Wang, The effect of nonequilibrium entropy production on the quantum fisher information and correlations, *Quantum Information Processing* **21**, 1 (2022).
- [58] K. Zhang, W. Wu, and J. Wang, Influence of equilibrium and nonequilibrium environments on macroscopic realism through the leggett-garg inequalities, *Physical Review A* **101**, 052334 (2020).
- [59] Y.-N. Zhou, T.-G. Zhou, and P. Zhang, Universal properties of the spectral form factor in open quantum systems, arXiv preprint arXiv:2303.14352 (2023).
- [60] M. Zwolak and G. Vidal, Mixed-state dynamics in one-dimensional quantum lattice systems: A time-dependent superoperator renormalization algorithm, arXiv preprint cond-mat/0406440 (2004).
- [61] A. Kulkarni, T. Numasawa, and S. Ryu, Lindbladian dynamics of the sachdev-ye-kitaev model, *Physical Review B* **106**, 075138 (2022).
- [62] P. Zhang, Y. Gu, and A. Kitaev, An obstacle to sub-ads holography for syk-like models, *Journal of High Energy Physics* **2021**, 1 (2021).